2008-06-11

An Optimization-Based Framework for Designing Robust Cam-Based Constant-Force Compliant Mechanisms

John Christian Meaders
Brigham Young University - Provo

AN OPTIMIZATION-BASED FRAMEWORK FOR DESIGNING ROBUST CAM-BASED CONSTANT-FORCE COMPLIANT MECHANISMS

by

John C. Meaders

A thesis submitted to the faculty of

Brigham Young University

in partial fulfillment of the requirements for the degree of

Master of Science

Department of Mechanical Engineering

Brigham Young University

August 2008

BRIGHAM YOUNG UNIVERSITY

GRADUATE COMMITTEE APPROVAL

of a thesis submitted by

John C. Meaders

This thesis has been read by each member of the following graduate committee and by majority vote has been found to be satisfactory.

Date	Christopher A. Mattson, Chair
Date	Larry L. Howell
Date	Spencer P. Magleby

BRIGHAM YOUNG UNIVERSITY

As chair of the candidate's graduate committee, I have read the thesis of John C. Meaders in its final form and have found that (1) its format, citations, and bibliographical style are consistent and acceptable and fulfill university and department style requirements; (2) its illustrative materials including figures, tables, and charts are in place; and (3) the final manuscript is satisfactory to the graduate committee and is ready for submission to the university library.

Date

Christopher A. Mattson
Chair, Graduate Committee

Accepted for the Department

Matthew R. Jones
Graduate Coordinator

Accepted for the College

Alan R. Parkinson
Dean, Ira A. Fulton College of
Engineering and Technology

ABSTRACT

AN OPTIMIZATION-BASED FRAMEWORK FOR DESIGNING ROBUST CAM-BASED CONSTANT-FORCE COMPLIANT MECHANISMS

John C. Meaders

Department of Mechanical Engineering

Master of Science

Constant-force mechanisms are mechanical devices that provide a near-constant output force over a prescribed deflection range. This thesis develops various optimization-based methods for designing robust constant-force mechanisms. The configuration of the mechanisms that are the focus of this research comprises a cam and a compliant spring fixed at one end while making contact with the cam at the other end. This configuration has proven to be an innovative solution in several applications because of its simplicity in manufacturing and operation.

In this work, several methods are introduced to design these mechanisms, and reduce the sensitivity of these mechanisms to manufacturing uncertainties and frictional effects. The mechanism's sensitivity to these factors is critical in small scale applications where manufacturing variations can be large relative to overall dimensions, and frictional forces can be large relative to the output force.

The methods in this work are demonstrated on a small scale electrical contact on the order of millimeters in size. The method identifies a design whose output force is 98.20% constant over its operational deflection range. When this design is analyzed using a Monte

Carlo simulation the standard deviation in constant force performance is 0.76%. When compared to a benchmark design from earlier research, this represents a 34% increase in constant force performance, and a reduction from 1.68% in the standard deviation of performance. When this new optimal design is evaluated to reduce frictional effects a design is identifed that shows a 36% reduction in frictional energy loss while giving up, however, 18.63% in constant force.

ACKNOWLEDGMENTS

I wish to express my thanks to Dr. Christopher Mattson for his direction and counseling throughout my research experience. Without his support this work could not have been completed. I also wish to thank Dr. Larry Howell and Dr. Spencer Magleby for their support and instruction, along with all the faculty of the Mechanical Engineering Department who stand out as examples of academic excellence and integrity.

This work was funded by the Brigham Young University Mechanical Engineering Department. ATL technology has generously shared practical insight, which helped make this research more meaningful. The students of the Compliant Mechanisms Research lab have also been a great support to me during my research work, and many have contributed solutions to difficult problems I have encountered in the research. Mostly I give thanks to my wife April who has spent many hours with me in the research lab, and supported me throughout my education.

Table of Contents

List of Tables

List of Figures

Nomenclature

α_i	The angle between two adjacent elements
a	Constant used to define an elliptical cam profile
b	Constant used to define an elliptical cam profile
B	A vector of constants that represent limits on constrained values
C	Percent constant force
$\hat{C}$	Surrogate model approximation of the percent constant force
δ	An increment of the total prescribed displacement
Δ	Total prescribed displacement
d_{ij}	Minimum distance between the i-th element and the j-th element
ε_i	Distance from the i-th node to the cam surface
ε_n	Gap distance (if positive) or interference (if negative) between mating parts
e	Number of elements
E	Young's Modulus
E_f	Energy loss due to friction
E_f^*	Optimized energy loss due to friction
F	Output reactionary force of the mechanism
F_f	Tangential friction force at the cam surface
F_l	Lower limit on allowable reaction force
F_u	Upper limit on allowable reaction force
γ_0	Force transmission angle between the cam and the compliant member in the initial position
γ_d	Force transmission angle between the cam and the compliant member in the fully deflected position
Γ_x	Size of the design domain in x direction
Γ_y	Size of the design domain in y direction
h	Cross sectional height of the compliant member
θ_c	Angle from the horizontal to the simulated crank
J	Aggregate objective function value for the multi-objective optimization
k	Vector of coefficients for the surrogate models
L_i	Length of the i-th element
μ	Coefficient of friction
n	Number of nodes
N	Normal force at the cam surface
p	Vector of design constants
r	Radius used to define an elliptical cam profile
r_c	Radius used to define a circular cam profile
R_i	Distance from the i-th node to the cam center

σ	Maximum bending stress in the compliant member
s	Number of displacement load substeps in the finite element analysis
s_c	Standard deviation of C
S_F	Safety Factor
S_y	Yield Strength
u	Vector of significant uncertain variables and parameters
U	Vector of all uncertain variables and parameters
ν	Poisson's ratio
v	Vector of design variables
w	Cross sectional width of the compliant member
W_i	Weight applied to the i-th objective in an aggregate function
x_c	Coordinate of the cam center in the x direction
x_i	Coordinate of the i-th node in the x direction in the initial position
x_{id}	Coordinate of the i-th node in the x direction in the fully deflected position
y_c	Coordinate of the cam center in the y direction
y_i	Coordinate of the i-th node in the y direction in the initial position
y_{id}	Coordinate of the i-th node in the y direction in the fully deflected position

Chapter 1

Introduction

1.1 Problem Statement

Constant-force mechanisms are a developing technology that has already been used in many systems where a variable output force is undesirable. One example of such a system is a robot arm for gripping fragile parts. In this system, an excessive gripping force can cause damage to the parts, but a minimum gripping force is required for the system to function. This means that the magnitude of the force must remain between these two limits during the system's operational motion. A constant force mechanism can provide a relatively constant output force for a large range of motion, making them useful in applications, such as the robotic gripper.

One particular constant-force mechanism design makes use of a flexible member attached to a base at one end while making contact with a cam surface at the other as shown in Figure 1.1. This design has been useful in many applications since it has a low part count, and the geometry is relatively simple. However, factors such as uncertainty in the geometry and uncertainty in the interaction between the compliant member and the cam surface, along with frictional effects, can present a significant difficulty in implementing the design. This thesis presents a design methodology that results in mechanisms with a high constant-force performance, a methodology for modeling and reducing sensitivity to manufacturing uncertainties, and a methodology for modeling and reducing the negative effects of friction on the design.

This thesis is divided into five chapters. Chapter 1 provides background and historical information regarding constant-force mechanisms. Chapters 2 and 3 develop models and optimization formulations for designing robust constant-force mechanisms. Chapter 4

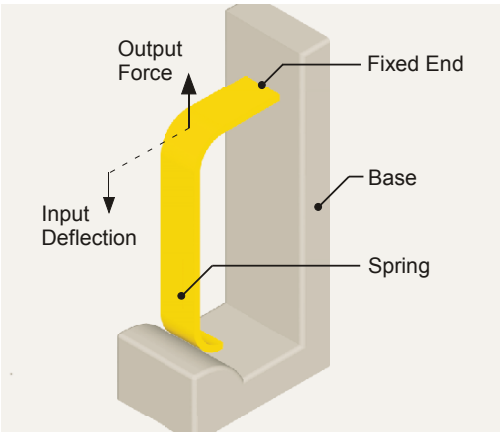

Figure 1.1: One possible configuration for a constant force mechanism.

presents the method for reducing frictional effects. These chapters have been developed as separate peer reviewed publications [2, 3, 4, 5]. Chapter 5 gives some concluding remarks and recommendations for future research.

1.2 Background

Most traditional springs have a linear force-displacement relationship. In many cases this is desired and useful. In some cases, as mentioned in the last section, such as mechanisms for gripping fragile parts or for end-effectors that cut glass, a consistent force over a sizable range of displacements is beneficial [6, 7]. Figure 1.2(a) compares these two types of force-displacement relationships. Springs that maintain a consistent force throughout a sizable displacement are known as constant-force springs. Constant-force springs can be designed using traditional kinematic analysis or by using more recent developments in the area of compliant mechanisms [8]. These compliant mechanisms are kinematic mechanisms that gain some or all of their motion by the large flexing of one or more of their members.

One class of constant-force springs, modeled after a slider-crank mechanism, is the focus of this thesis. Figure 1.3 illustrates the mechanism and how it is used to represent a constant-force spring. Figure 1.3(a) shows the conventional slider-crank constant-force mechanism. The constant-force attribute of this design comes from carefully managing the stiffness of the compliant member and its alignment with the crank. As the input deflection

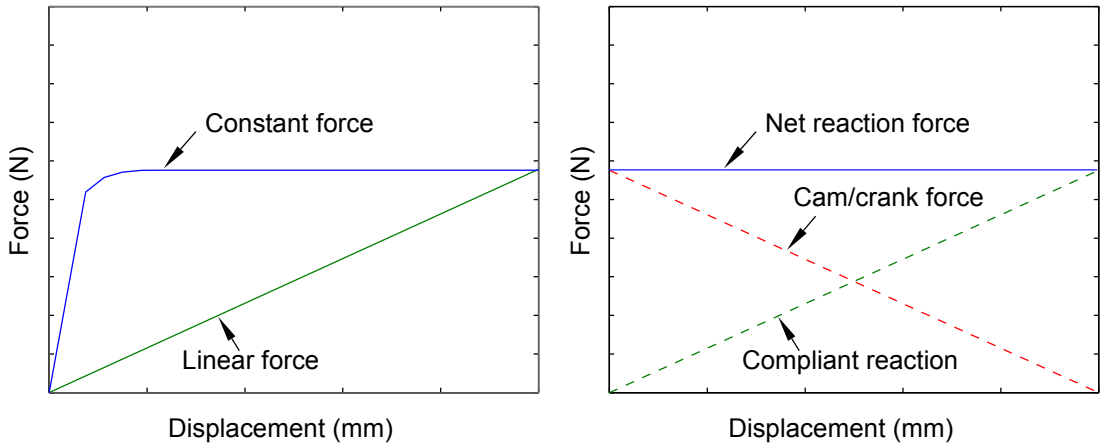

Figure 1.2: Force-displacement curve for a constant-force spring. (a) Comparison of a constant-force spring to a linear spring. (b) The components of reaction force that result in a constant-force net reaction.

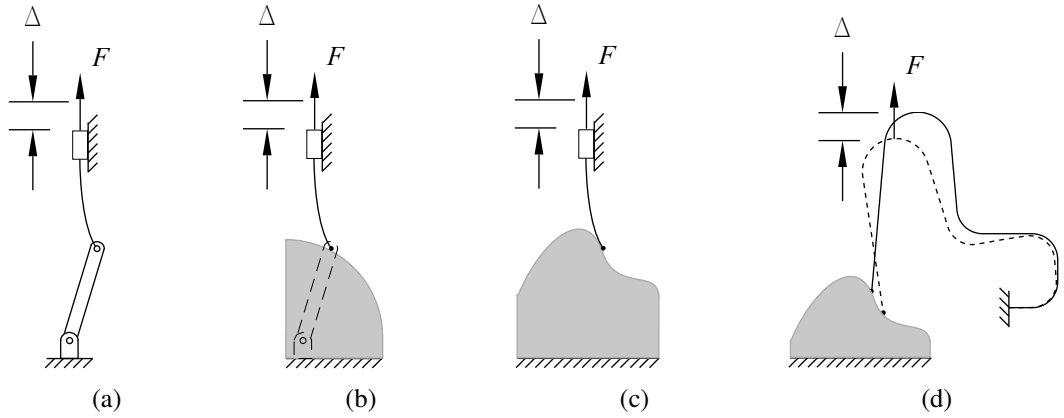

Figure 1.3: Side view of a constant-force slider-crank mechanism with simulated pin joint variations showing the input deflection (Δ) and the ouput force (F). (a) Basic slider-crank with a pinned-pinned rigid link. (b) A Pinned-Pinned rigid link (shown as broken lines) simulated by a circular cam. (c) An arbitrary cam in place of the circular cam. (d) Geometry of an electrical contact in place of the slider.

is increased, the compliant member is flexed and gives an increasing reaction force to the deflection. The reaction force that is transmitted from the crank, however, is decreasing due to a changing force transmission angle. Figure 1.2(b) shows a force-deflection plot with these forces and the resulting net force.

Figure 1.3(b) shows a variation of the slider-crank mechanism with a cam replacing the crank. In many applications, especially small scale applications, this cam design is more manufacturable than one with a pinned rigid link. The cam in this variation of the slider-crank mechanism is a simulated pin joint because the end of the compliant member mimics the motion of the pinned version as it follows the cam surface. Some of the difficulties and assumptions in using a simulated pin joint can be found in [1]. A circular cam profile, as shown in Figure 1.3(b), can be used to match the motion of a rotating rigid link. Other, non-circular, profiles may be beneficial to the performance of the mechanism. The simulated pin joint with an arbitrary cam profile is shown in Figure 1.3(c).

For some applications, the slider portion of the mechanism can also be difficult to implement. In these cases a design such as the one shown in Figure 1.3(d) can be used. In this design a vertical deflection is still applied, but the motion is not strictly restricted in the horizontal direction as it is with a slider. Instead, the multiple-bend compliant member can deflect as needed to achieve the desired vertical deflection, or even a desired horizontal deflection.

While this configuration simplifies the manufacturing process, it presents new challenges in the design process. The multiple-bend spring must be designed with manufacturing limitations and yielding conditions in mind, while at the same time manipulating its interaction with the cam to control the variability in the output force. In addition to these difficulties, manufacturing uncertainties and frictional forces developing at the cam surface can significantly alter the mechanisms performance. As mentioned before, the purpose of this thesis is to present a design methodology that includes a consideration of manufacturing uncertainties and frictional sensitivities.

The examples used in this thesis come from the design of electrical connectors. When designing electrical connectors the magnitude of the force that develops between the two connecting electrical devices (called the contact normal force) is of interest. This force relates to the electrical connection and is different than the normal force that develops between the cam and the compliant member. A large contact normal force can cause excessive part wearing, and a small contact normal force results in high electrical resistance [1]. Many connectors rely on deflected cantilever-type or pogo-type contacts to generate the

contact normal force. As such, the magnitude of the force has a linear relationship with the deflection of the contact. Ideally, the deflection of the contact can be controlled to keep the contact normal force at a desirable magnitude, but smaller scale devices and possible dynamic operating conditions make this control difficult in practice. The problem is worsened when connectors with an array of contacts are considered, because each contact will deflect differently than the other contacts in the array due to dimensional and assembly uncertainties. This makes the electrical resistance for each contact different. Because of these difficulties, a constant-force electrical contact would be useful. The size of electrical contacts restricts the level of complexity allowed in their design making it necessary to have a simple configuration, such as the one discussed earlier and show in Figure 1.3(d).

1.3 Literature Review

This section reviews previous work in the development of constant-force systems, and compliant mechanisms as well as work done to make these devices more robust.

Various mechanical systems have been used in the past to achieve a constant output force for a given range of input displacements. Complex algorithms and feedback loops coupled with pneumatic, hydraulic, and electrical actuators have been used to achieve a desired constant force performance [9, 10]. While effective, these constant force systems can be expensive to implement and maintain, and are not easily scaled to very small devices. These strategies are therefore prohibitive when considered for tiny mass produced devices such as electrical contacts [1].

Recently, constant-force *mechanisms* have been used as a significantly less expensive way to achieve constant output force over a desired deflection range. Nathan [9] developed a constant-force mechanism that is commonly found in desk lamp stands that supports the lamp in any position. Nathan's mechanism is a chain of parallel mechanisms and linear springs that support a mass regardless of the mass' position relative to the mechanism. The work by Nathan was more recently extended by Herder et al. [11] when they developed four and six degree-of-freedom mechanisms with larger ranges of motion than Nathan's chain of parallel mechanisms. Additionally, Jenuwine and Midha have designed a constant-force mechanism for concrete testing [12].

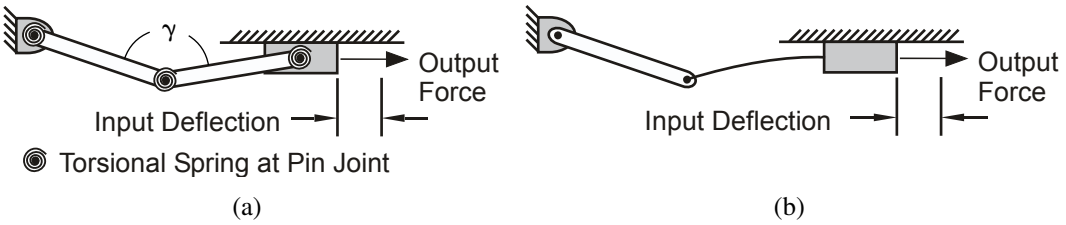

Figure 1.4: (a) Compression-type constant force mechanism with rigid links and torsional springs at pin joints. (b) Configuration of a compliant constant force mechanism with flexible and rigid links.

Most recently, *compliant* constant-force mechanisms have been introduced as a means to reduce part-count and increase precision over rigid-body mechanisms [13]. Compliant mechanisms gain some or all of their motion from the deflection of flexible members as opposed to movement of rigid links connected by pin joints [8]. Evans and Howell have designed compliant constant-force robot end-effectors [7]. Howell and Magleby have designed and patented exercise equipment based on compliant mechanism constant-force technology [14]; and Weight et al. have developed constant-force electrical contacts [1], albeit from a deterministic development. Nahar and Sugar consider the design of micro compliant constant force mechanisms [6].

Various developments have been made that make the general modeling and design of compliant constant force mechanisms easier. Among the most useful developments is the Pseudo Rigid Body Model (PRBM); a model used to analyze compliant mechanisms using equations from rigid-link mechanisms [8]. The PRBM significantly reduces the complexity of analysis, and is particularly useful in the early phases of design where appropriate geometric configurations must be determined to assure that a mechanism will achieve the required motion.

One of the most common approaches for modeling a constant-force mechanism is as a traditional slider-crank mechanism with torsional springs at some or all of the joints. Such a mechanism is shown in Figure 1.4(a). The constant force behavior of this mechanism is due primarily to two factors. The first is the decreasing force transmission angle (γ) between the two long links in the figure, and the second is the increasing spring force as the torsional spring deflects. To design constant force mechanisms based on this model, a

designer must select geometry, and torsional spring constants that balance the decreasing transmission angle and the increasing spring force. [8] Figure 1.4(b) shows a compliant constant-force slider-crank mechanism, which is the same configuration shown earlier in Figure 1.3(a).

Murphy et al., developed a type-synthesis framework for designing compliant constant force mechanisms based on the slider-crank model. [15]. Twenty-eight possible configurations for the compliant constant force slider crank mechanism, identified by Murphy et al. and have been further developed by various researchers. [8, 13, 16, 17] Optimization techniques have been developed using a finite element analysis to identify appropriate geometry and spring constants for maintaining a constant force with these slider-crank mechanisms. This is similar to the deterministic design approach used in this thesis. [18]

The deterministic approach for constant-force electrical contact design used by Weight et al. builds on these developments. In their work, Weight et al. discuss many of the challenges faced when using the simulated-pin-joint configuration to develop a constant-force electrical contact, and solutions to overcome them. In their analysis the cam is modeled as the traditional rigid link. This, however, leads to some limitations in the model. Some of the problems identified in the model include: a pinned link supporting tension when the cam surface cannot apply tension on the spring, unmodeled frictional forces at the cam surface, and the deflection of the spring through the unmodeled cam surface. These limitations can be controlled through the use of constraint functions during the design optimization routine. The developments in the publication did not include a method of handling geometric uncertainty which is a key component of this thesis. As a result of the work presented by Weight et al. several electrical contact prototypes were manufactured and tested. Figure 1.5 shows a constant-force electrical contact prototype. This prototype outputs a force that is 73.20% constant over its operational range. This performance value is used as a benchmark comparison for several of the examples in this thesis. [1]

Taguchi [19] developed and presented a method for robust design. Many researchers have since further developed Taguchi's method and have created new methods for robust design [20, 21]. Optimization methods have been developed to identify robust optimal designs [22]. Response surface approximations and surrogate models are common methods

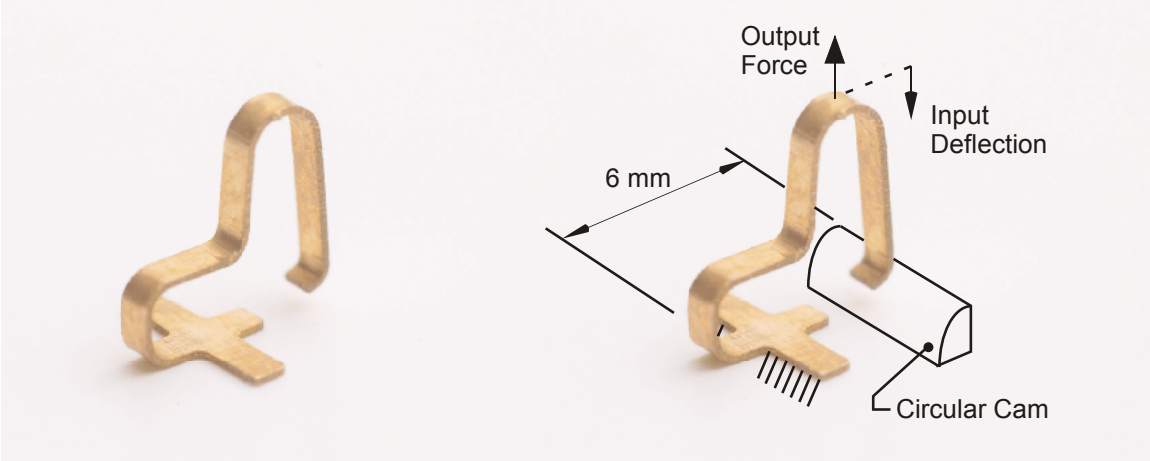

Figure 1.5: Prototype of a constant-force electrical contacts made by Weight et. al [1]

currently used in robust design optimization. Simpson et al. [23] explore the use of different surrogate modeling approaches and their application to engineering design. Wittwer et al. apply several uncertainty analysis methods to micro-compliant mechanisms [24]. The analysis of the mechanisms studied by Wittwer et al. is similar to the analysis of constant force mechanisms because both exhibit nonlinear behavior.

There have been many methods developed to reduce the negative effects of friction on a system. In many aerodynamic applications the shape of a part is altered to reduce the drag from skin friction [25]. In control systems, it is often useful to model friction and then compensate for the difference it makes in the motion of the system. Olsson et al. present several models for friction and a method for friction compensation [26]. Some research has also been done in frictional analysis for compliant constant-force mechanisms. Boyle et al. examine the effect friction has on a slider-crank constant-force mechanism, and develop a model to predict the dynamic force-deflection relationship with those effects. This model uses the Pseudo-Rigid-Body Modeling technique and the principle of virtual work with Coulomb friction to determine the force-deflection relationship of the mechanism. The model is calibrated and validated with prototype tests, however the model is not used during the design phase of the prototypes. [27]

In three recent publications work was done to design robust constant-force mechanisms [2, 3, 4]. The developments and results of these publications are included in this

thesis as Chapters 2 through 4. Each of the publications takes a step toward developing a design strategy for robust mechanisms with reduced frictional effects.

Chapter 2

Mating Condition Uncertainty

This chapter presents the initial steps toward robust optimization of constant-force mechanisms based on the methodology developed in [2]. It begins with the development of the finite element model used in all the following optimization formulations. It then develops both a deterministic and a robust design optimization formulation. The robust formulation is based an evaluation of the mating condition. A Monte Carlo simulation is used to evaluate the sensitivities of both solutions. In this chapter, circular cams are modeled using a pinned-pinned rigid link in the analysis.

2.1 Constant-Force Mechanism Model and Optimization

In this section we present the models used to design and optimize the compliant constant-force mechanism. We begin, in Section 2.1.1, by describing a geometric model that is used to define the design, which gives additional design freedom not included in some previous design methods. Section 2.1.1 also gives a description of the method used to model geometric uncertainty. In Section 2.1.2 a description of how the force, displacement, and stress relationships are modeled is provided. Sections 2.1.3 and 2.1.4 provide deterministic and non-deterministic optimization problem statements, respectively.

2.1.1 Modeling the Design Domain

This section presents the geometric model used to define the mechanism; a definition which is used during the optimization process. The two dimensional model depicts the mechanism from its side view in the design domain, which is shown as a shaded area in Figure 2.1. The design domain, as defined by dimensions Γ_x and Γ_y, encloses the complete

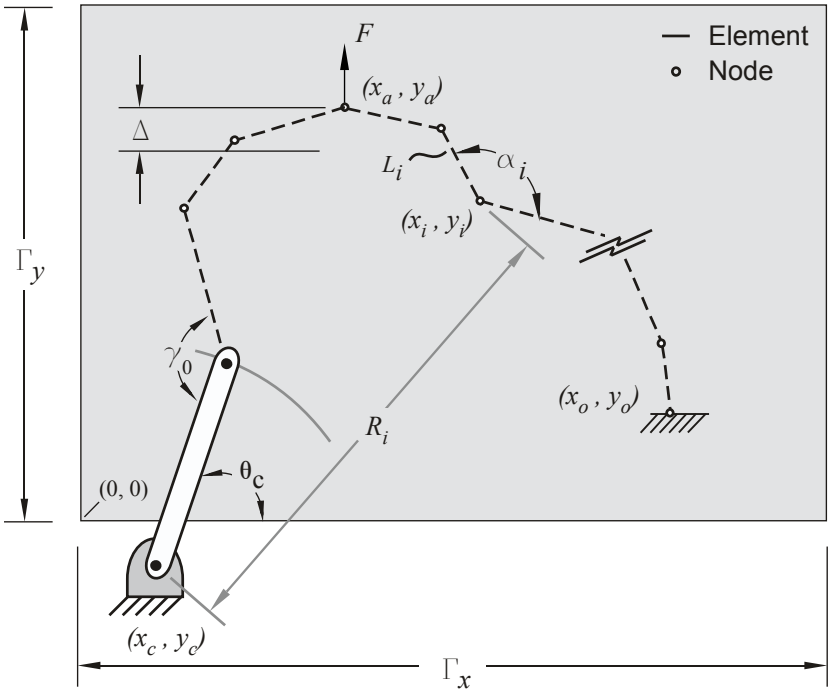

Figure 2.1: Design domain and associated variables and parameters.

mechanism geometry, with the exception of the cam center, which is permitted to occupy any point in the two-dimensional space.

Unlike the geometric model from earlier work [1], the design domain model uses the Cartesian coordinates of each node (x_i, y_i) as variables for the design optimization. Because the nodal coordinates are permitted to be anywhere within the design domain, the optimization has nearly complete freedom to search for constant force configurations. Two nodes, however, must remain at fixed positions in order to preserve predetermined mating with other devices (i.e., a circuit board, another electrical device). These nodes are at the point (x_o, y_o) where the mechanism is fixed to the base, and at the point (x_a, y_a) at which the deflection (Δ) is applied. The total number of nodes (n) and elements (e) in the design is chosen according to the desired resolution of the finite element model.

Importantly, we note that the end of the cam link (x_c, y_c), in Figure 2.1, is not restricted to be within the design domain. We simply use the cam link to simulate an actual cam that will be used in the physical implementation of our design. Therefore, the center of curvature for the cam is not required to be within the design domain.

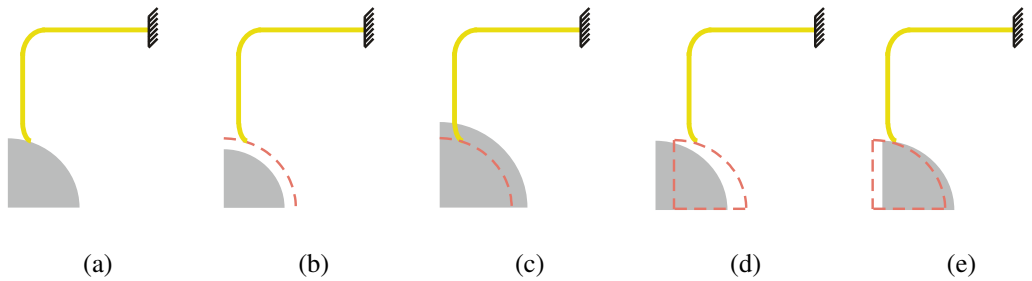

Figure 2.2: Significant geometric uncertainties for simulated pin joints. (a) Ideal case. (b) Cam radius too small. (c) Cam radius too big. (d) Cam and spring not fully assembled. (e) Cam and spring over assembled.

Figure 2.1 also illustrates variables that are used to formulate behaviorial constraints that ensure that the resulting design will be both manufacturable, and within the predictive capabilities of the simulated pin joint model. Specifically, we define the angle between two adjacent elements (α_i), the length of each element (L_i), the distance from each node to the cam center (R_i), the angle between the cam link and the preceding element (γ_0), and the angle between of the cam link as measured from the horizontal (θ_c).

Modeling Geometric Uncertainty

The geometric model described above is sufficient for deterministic optimization. We wish, however, to reduce the effect of uncertainties that are known to exist but are not modeled above. In the following, we describe and model two general sources of uncertainty in our constant-force mechanism model. One source of uncertainty arises from variations in our design variables and parameters. To characterize the robustness of a particular design with respect to the variables and parameters we use a Monte Carlo simulation to create a population of mechanisms with normally distributed random values, and determine the percentage of constant force for each one. We use the standard deviation (s_c) of the constant force percentage to determine the degree to which a design is robust.

The second source of uncertainty arises from different mating conditions between the assembled mechanism parts (spring and cam) that may be encountered. Several possible mating scenarios are illustrated in Figure 2.2. The first case, shown in Figure 2.2(a), is an ideal case where the spring and the cam mate exactly as designed by the geometric model

above. In this case, the geometric model without variation is sufficient. The second case, shown in Figure 2.2(b), occurs when the cam is manufactured with a smaller radius than the nominal value. This results in a gap between the cam and the spring, and the interaction between the two will not occur until the deflection of the spring closes this gap. The third, shown in Figure 2.2(c), occurs when the actual cam radius is larger than the nominal value. In this case, the cam will deflect the spring during assembly, and the spring may behave differently during the operational deflection. The fourth and fifth cases, shown in Figures 2.2(d) and 2.2(e) respectively, both involve variations in assembly. For both cases the cam and beam geometry are exact, but in Case 4 the mechanism is not fully assembled which increases the distance between the cam center and the fixed point, and in Case 5 the mechanism is over assembled which decreases the distance between the cam center and the fixed point. Case 4 results in a gap and Case 5 results in an interference similar to the second and third cases. All of the various mating possibilities can be categorized into three basic modes: an exact mating, a mating gap, or a mating interference.

For a mechanism that has a gap between the mating parts, we adjust the geometric model by essentially removing the pin joint and allowing the end of the metallic beam to move unconstrained until it reaches the cam surface. At each step of the load analysis the size of the gap is tested to see if contact is made. When contact is made the pin joint is reactivated and the mechanism geometry is as before.

When the mating condition is an interference condition we must determine the deflection and stresses that are created during assembly before applying the operational deflection. We do this by starting the cam in a position where the interference is removed and then applying several displacement steps to the cam center to move the cam back to its original position. This will deflect the compliant member as if the mechanism were being assembled. We use this deflected position and the corresponding stresses as our initial condition when we apply the preload and operational deflection. The next section discusses the methods we use to determine the deflections and stresses in the designed mechanism.

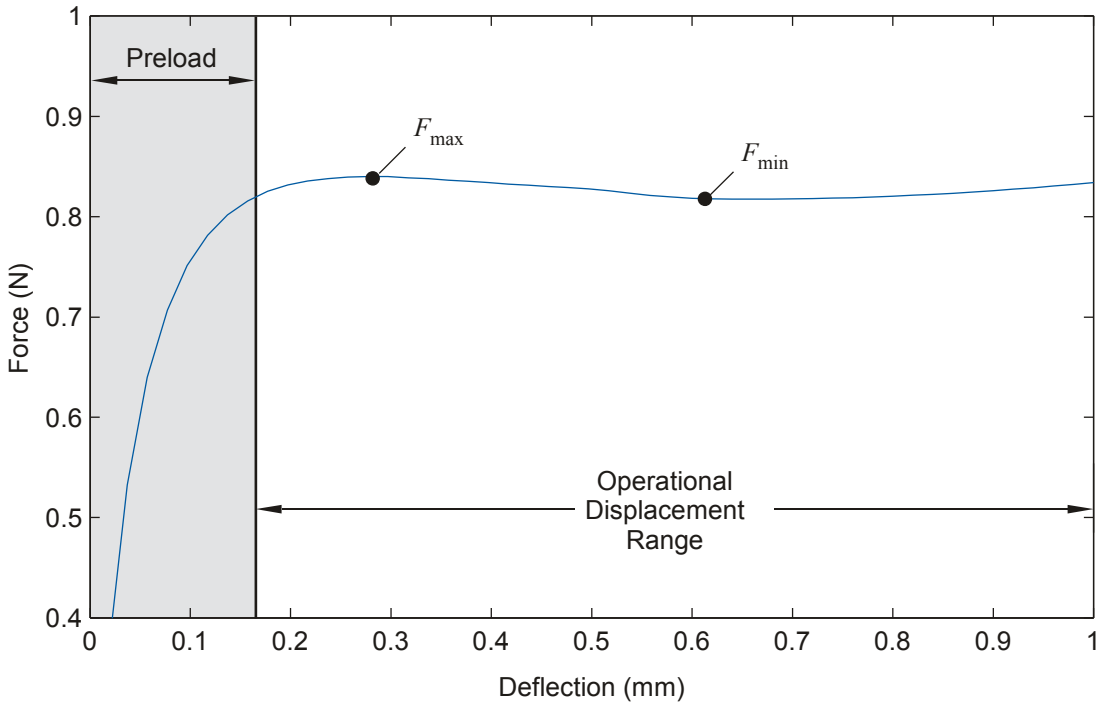

Figure 2.3: Generic force-displacement curve for a constant force device.

2.1.2 Modeling Force, Displacement, and Bending Stress Relationships

We use a finite element method to determine the force-deflection relationship of the mechanism, and to determine the internal stresses caused by the deflection. We model each element of the spring as a beam element using the Timoshenko beam theory [28]. Because this mechanism undergoes large nonlinear deflections, nonlinear methods are used to solve the beam equations for nodal displacements. We use a Newton-Raphson iteration method to converge on a nodal solution after providing an initial guess of nodal displacements [28]. The internal stresses and the reaction forces are calculated directly from the beam equations once the solution is known. One difficulty with the Newton-Raphson iteration is that it can diverge if the initial guess is too far from the solution. To prevent this we apply the total deflection (Δ) to the mechanism in many small increments (δ).

These increments become data points for constructing the force deflection curve. The force-deflection curves of constant-force mechanisms typically have a region where the force increases steeply with increasing deflection followed by a nearly flat region. A typical curve is shown in Figure 2.3. As seen in the figure, a small preload is applied to

avoid the region of steep force increase. This preload deflects the mechanism beyond the region of increasing force, so that the deflections that occur during operation are in the flat region. When determining the level of constant force for the mechanism we consider only the variation in force over the operational displacement range. The level, or percentage, of constant force is related to the maximum and minimum forces in that range by Equation 2.1

$$C = 100\frac{F_{min}}{F_{max}} \tag{2.1}$$

The interested reader is referred to the appendix of this thesis where a description of the analysis code is presented. This section has presented the models used to characterize the performance of the constant force mechanism and the performance uncertainty due to variations in cam/beam mating. The following two sections use these models in optimization problems to identify mechanism geometry that results in a constant force output.

2.1.3 Deterministic Optimization Formulation

In this section we present the deterministic optimization problem statement used to find the optimal geometry that produces a constant force over a large prescribed deflection range. The constraints developed in this section will also be used in the robust design optimization problem statement of Section 2.1.4, but will be altered to ensure that uncertain conditions do not lead to violated constraints.

Equations 2.2 to 2.14 define the optimization problem that is used to design a constant-force mechanism.

$$\max_{v} C(v,p) \tag{2.2}$$

subject to

$$F_{\max} \leq F_u \tag{2.3}$$

$$F_{\min} \geq F_l \tag{2.4}$$

$$d_{ij} > 0 \qquad (i,j = 1,2,...,e, j > i+1) \tag{2.5}$$

$$\alpha_i \geq \alpha_{\min} \qquad (i = 1,2,...,e-1) \tag{2.6}$$

$$L_i \geq L_{\min} \qquad (i = 1,2,...,e) \tag{2.7}$$

$$\gamma_0 < \gamma_{max} \tag{2.8}$$

$$\gamma_d \geq \frac{\pi}{2} \tag{2.9}$$

$$0 < \theta_c < \pi/2 \tag{2.10}$$

$$R_i \geq r_c \qquad (i = 1,2,...,n-2) \tag{2.11}$$

$$\sigma \leq \frac{S_y}{S_F} \tag{2.12}$$

$$0 \leq x_i \leq \Gamma_x \qquad (i = 1,2,...,n) \tag{2.13}$$

$$0 \leq y_i \leq \Gamma_y \qquad (i = 1,2,...,n) \tag{2.14}$$

where p is a set of designer specified design parameters listed in Table 2.1, and v is a set of design variables including all the nodal locations, the cam radius, and the cam center location. As seen by Equation 2.2, the objective of this optimization is to maximize the percent constant force that the mechanism outputs. Equations 2.3 and 2.4 keep the maximum output force below an upper limit and the minimum output force above a lower limit. Equation 2.5 is included in the problem statement to keep the string of elements from crossing over itself. Equations 2.6 and 2.7 limit the angle between adjacent elements and restricts the minimum length of the elements, respectively. These constraints are included in the statement to keep the search for constant force mechanisms practical from a manufacturing perspective. Equations 2.8 and 2.10 keep the cam link angles within the capabilities of the simulated pin joint model, and Equations 2.9 and 2.11 keep the nodes and elements of the mechanism from passing through the cam surface or trying to occupy any space where the cam physically exists. Stress is maintained under control by Equation 2.12. Finally, the nodal locations, which are completely free to move during the optimization search, are required to say within the design domain as specified by Equations 2.13 and 2.14. Again, we note that the cam center is allowed to freely move to any position in space.

Table 2.1: Parameter Description for Deterministic Optimization

Parameter	Description
x_o	x Coordinate of Fixed Point
y_o	y Coordinate of Fixed Point
x_a	x Coordinate of point where force is applied
y_a	y Coordinate of point where force is applied
n	Number of nodes
E	Young's Modulus
ν	Poisson's Ratio
w	Cross section width
h	Cross section height
Δ	Total deflection range including preload

2.1.4 Non-deterministic Optimization Formulation

The optimization problem formulation presented in this section is used to search for optimal mechanism geometry while trying to both maximize C and decrease variation in C across known tolerance windows. This problem is given in Equations 2.15 to 2.27.

$$\min_{v} -(C_L(v,p) + C_N(v,p) + C_U(v,p)) \tag{2.15}$$

subject to

$$F_{\max} \leq F_u - \tilde{F}_{\max} \tag{2.16}$$

$$F_{\min} \geq F_l + \tilde{F}_{\min} \tag{2.17}$$

$$d_{ij} > 0 + \tilde{d}_{ij} \qquad (i,j = 1,2,...,e, j > i+1) \tag{2.18}$$

$$\alpha_i \geq \alpha_{\min} + \tilde{\alpha}_i \qquad (i = 1,2,...,e-1) \tag{2.19}$$

$$L_i \geq L_{\min} + \tilde{L}_i \qquad (i = 1,2,...,e) \tag{2.20}$$

$$\gamma_0 \leq \pi - \tilde{\alpha}_c \tag{2.21}$$

$$\gamma_d \geq \frac{\pi}{2} + \tilde{\gamma}_d \tag{2.22}$$

$$0 + \tilde{\theta}_c \leq \theta_c \leq \frac{\pi}{2} - \tilde{\theta}_c \tag{2.23}$$

$$R_i \geq r_c + \tilde{R}_i \qquad (i = 1,2,...,n-2) \tag{2.24}$$

$$\sigma_{\max} \leq \frac{S_y}{\tilde{S}_F} \tag{2.25}$$

$$0 + \tilde{x}_i \leq x_i \leq \Gamma_x - \tilde{x}_i \qquad (i = 1,2,...,n-1) \tag{2.26}$$

$$0 + \tilde{y}_i \leq y_i \leq \Gamma_y - \tilde{y}_i \qquad (i = 1,2,...,n-1) \tag{2.27}$$

where C_L is the constant force percentage when the design is evaluated at the lower end of the tolerance window resulting in the smallest gap or largest interference, and C_U is the percentage of constant force when the design is evaluated at the upper end of the tolerance window resulting in the largest gap or smallest interference. C_N is the percentage of constant force at the nominal values.

From a practical point of view, Equation 2.15 searches for a mechanism design that performs well at the two extremes of our mating conditions and at the nominal mating condition. We can find the mating extremes because we know our tolerance window, and the mating condition is simply a function of the geometric parameters of the model. This strategy is somewhat similar to sampling strategies for robust design with two significant differences. First, we strategically select three points in the design space rather than select a large number of random samples, and second we directly optimize the performance at those three points rather than estimate a variance to optimize.

This is a simplified robust formulation, and it is important that we recognize the limitations of this method. While this method has a low computational expense compared to more thorough robust optimization methods, the optimum is not guaranteed to be more robust. We must verify the robustness of the optimum using a more thorough approach. We use a Monte Carlo simulation to do this by testing a sample of mechanisms within the tolerance limits of our optimum design.

As mentioned earlier, it becomes necessary to adjust the constraints to ensure that any mechanism within our tolerance window does not violate our constraints. Equations 2.16 to 2.27 show the adjusted form of the constraint equations. An additional term has been added to each constraint that reduces the design space by an amount (shown with a tilde) that is determined by the variance in each of the constrained values. Determining

an appropriate value for tightening the constraints can be difficult due to the dependence of many values on the finite element analysis. For constraints that depend only on the geometry of the design the constraint can be adjusted directly since we know what geometry our tolerance window will permit. For example, we know what limits our tolerances will allow on element lengths so we can directly adjust our constraint on the minimum element length such that no design will violate this constraint within a tolerance window. For a constraint such as the maximum allowable stress, however, we do not know what effect the tolerance window may have on the stress within the compliant member, since it depends on the finite element analysis. In this case we run a Monte Carlo simulation on a design, prior to optimizing, to determine the variance of the constrained finite element analysis values within our manufacturing tolerance limits. We then use this information to determine how much we must adjust the constraint during the optimization routine. Using this approach we must again check the optimum design to ensure that none of the original, or unadjusted, constraints is violated through variation in our design.

2.2 Numerical Results

This section presents two examples to demonstrate the optimization models developed in the previous section. We will compare the results of these two examples to see the difference in performance and robustness that occurs as a result of the different objective functions. We will also compare our results to the results obtained by Weight et al. [1] to observe the difference that occurs by using the design domain approach. For comparison purposes this benchmark design's geometry has been approximated from the published results and analyzed using the finite element model and Monte Carlo simulation described above. The results are shown in Figures 2.4 and 2.5(a). These results are slightly different from the published results due to the different method of analysis.

2.2.1 Deterministic Optimization and Robustness Check

The first example that we present is the design that results from the deterministic optimization statement. In this example we keep the assumption (only during the design

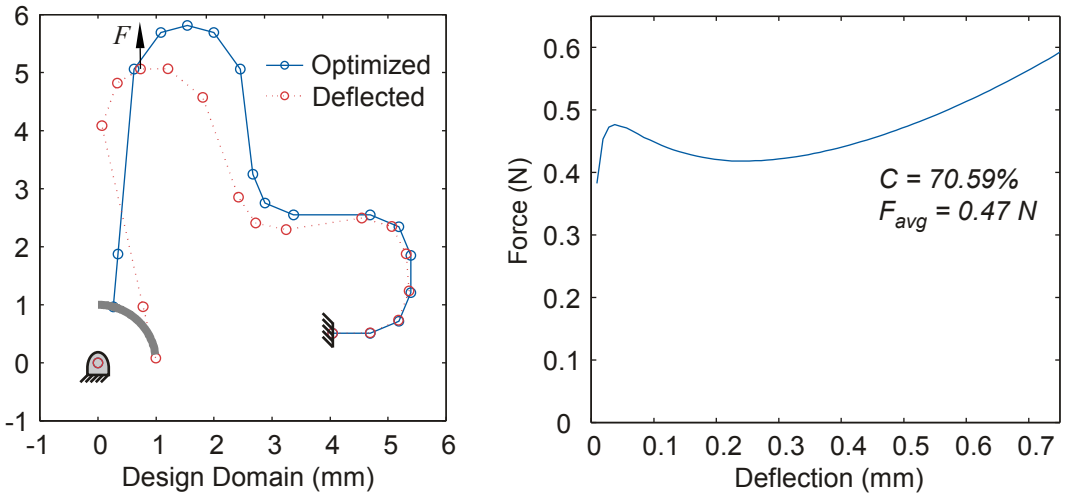

(a) (b)

Figure 2.4: The benchmark design. (a) Side view of the geometry with non-exaggerated deflected shape. (b) Force-deflection curve.

phase) that the spring and the cam will remain in contact. We then test this design using both sources of uncertainty discussed in Section 2.1 in a Monte Carlo simulation to evaluate its sensitivity to variation. Table 2.2 lists the fixed parameters that we use for this example. These values are selected to match the benchmark design [1], and all are in the range that could be considered when designing a constant-force-electrical mechanism.

The resulting design in its initial position and its deflected position is shown in Figure 2.6 with its corresponding force-deflection curve. The percentage of constant force for this design is 97.50%. We now do a Monte Carlo simulation on the design to determine the robustness of the deterministic results. In this simulation we will include uncertainty in all the design variables, and fixed values that we use for the finite element model. We also allow the mating condition to change depending on the random values of the other finite element inputs. For all the uncertain variables we use a normal distribution with a mean at the nominal value and a standard deviation equal to one third of the tolerance limit shown in Table 2.2. Figure 2.5(b) shows the distribution of constant force percentages for a sample of 1,000 mechanisms. The average percentage for the sample is 94.82% constant with a standard deviation of 2.46%. The next example reduces this standard deviation by implementing the non-deterministic optimization.

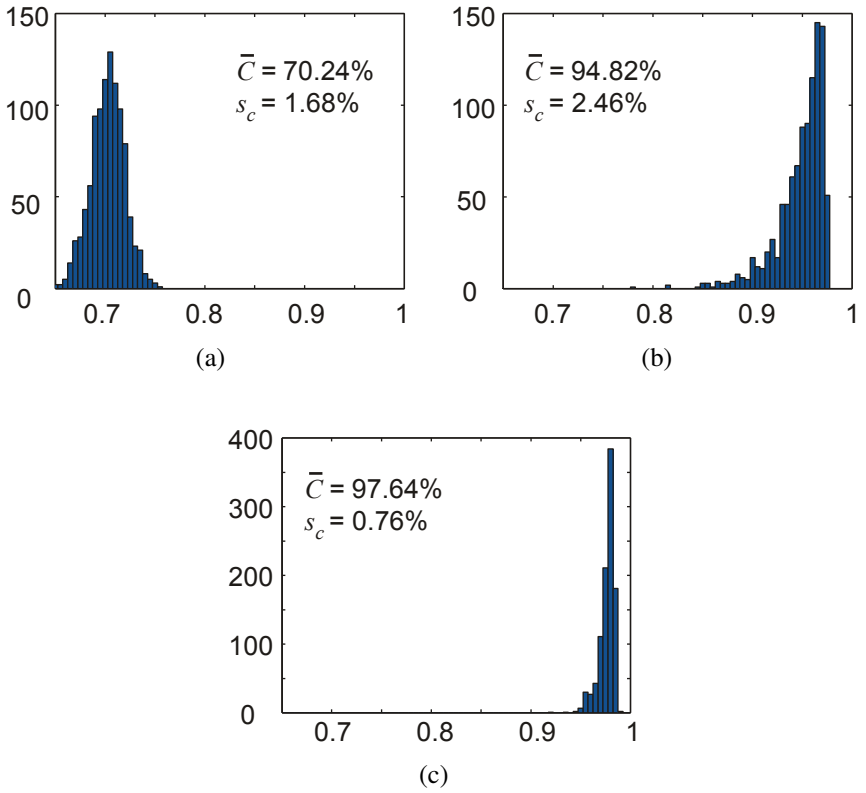

Figure 2.5: Monte Carlo results for three designs with 1,000 samples each. (a) Benchmark design. (b) Deterministic solution. (c) Non-deterministic solution.

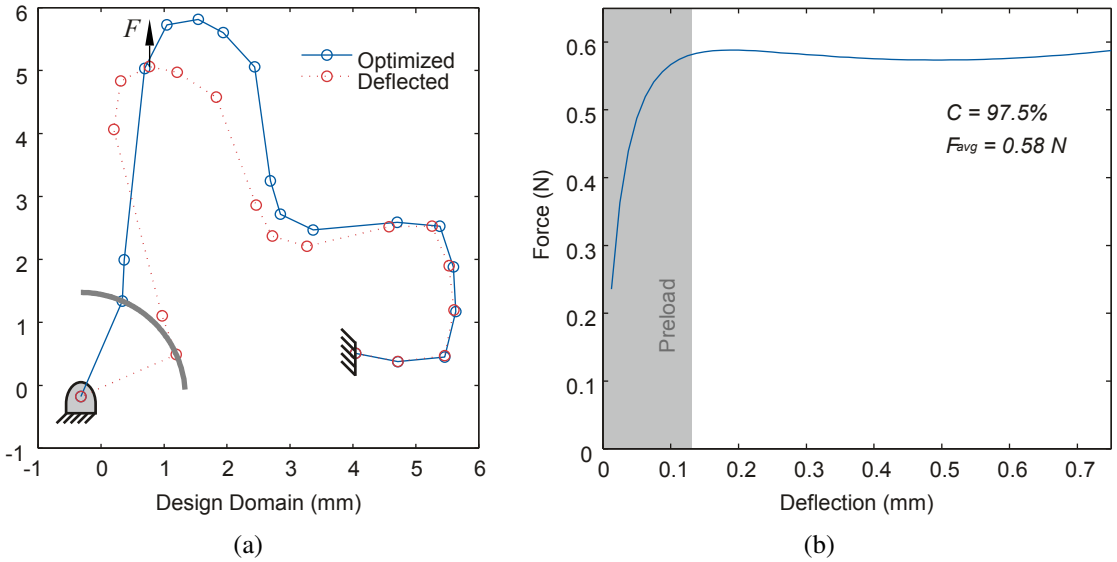

Figure 2.6: Deterministic Solution. (a) Side view of optimized geometry (nodal representation) with non-exaggerated deflected shape. (b) Force-deflection curve for optimized design.

Table 2.2: Fixed Parameter Values for Optimization

Parameter	Description	Value
x_o	x Coordinate of Fixed Point	4.04 mm
y_o	y Coordinate of Fixed Point	0.51 mm
x_a	x Coordinate of point where force is applied	1.54 mm
y_a	y Coordinate of point where force is applied	5.81 mm
n	Number of nodes	18
E	Young's Modulus	110 GPa
ν	Poisson's Ratio	0.34
w	Cross section width	1.00 mm
h	Cross section height	0.2 mm
Δ	Total deflection range including preload	0.75 mm
δ_p	Preload deflection	0.11 mm
S_F	Safety factor on stress	1.0
$\tilde{x}$	Tolerance limit on x	0.03 mm*
$\tilde{y}$	Tolerance limit on y	0.03 mm*
$\tilde{E}$	Tolerance limit on E	5.0 GPa*
$\tilde{\nu}$	Tolerance limit on ν	0.005*
$\tilde{w}$	Tolerance limit on b	0.03 mm*
$\tilde{h}$	Tolerance limit on h	0.03 mm*
$\tilde{r_c}$	Tolerance limit on r_c	0.03 mm*

*Typical values provided by ATL Technology

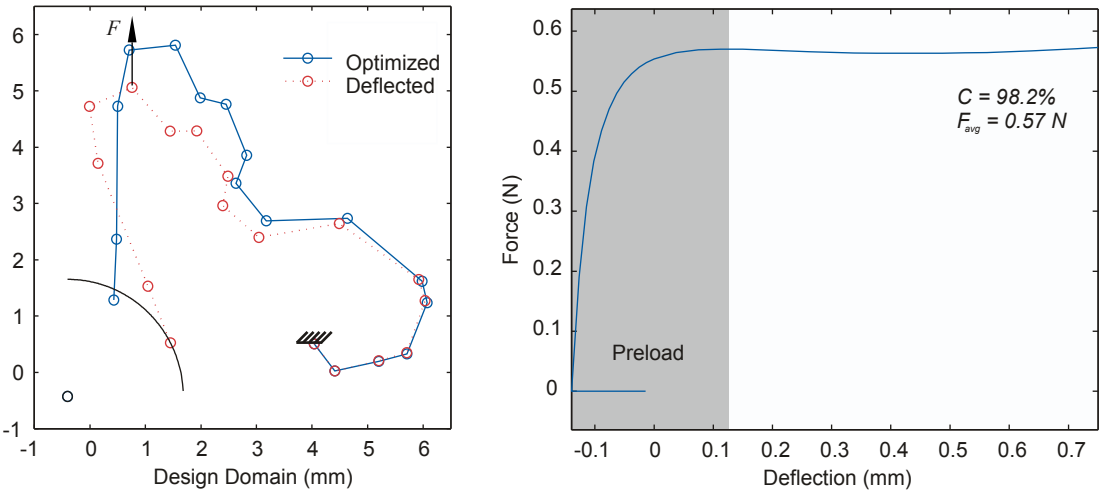

(a) (b)

Figure 2.7: Non-deterministic Solution. (a) Side view of optimized geometry (nodal representation) with non exaggerated deflected shap. (b) Force-deflection curve for optimized design.

2.2.2 Non-Deterministic Optimization and Robustness Check

We now present an example in which we eliminate the assumption (during the design phase) that the cam and the spring always stay in contact. We will use the same designer specified parameters as we did in the deterministic case, but in this case we will use the non-deterministic approach as presented earlier. Note that with the non-deterministic approach we are allowing the optimizer to intentionally design a gap or an interference between the spring and the cam.

Figure 2.7 shows the resulting design's geometry with the nominal mating condition and the corresponding force-deflection curve. The constant force percentage for this design is 98.20%. It may seem surprising that this percentage is higher than the deterministic solution since we have tightened the constraints and added two new objectives (C_L, C_U) to the formulation. As noted before, however, we are now allowing the optimizer freedom to design gaps or interference fits in the mechanism. A close inspection of Figure 2.7 shows that the new design has an interference fit, and the force-deflection curve has been shifted due to the initial assembly deflection that occurs. Since we will use the same operational displacement range we must apply a larger preload. This means that the force must remain constant over a smaller portion of the entire deflection range, and better designs can be found.

We use the same Monte Carlo simulation that we used in the previous section to determine the robustness of the non-deterministic solution, and the histogram is shown in Figure 2.5(c). We see from the histogram that the performance of this design is contained within a smaller region of variation. The average constant force percentage is 97.64%, with a standard deviation of 0.76%. We see that the new design improves both the average percentage and the standard deviation.

Before moving on we must also verify that our non-deterministic solution does not violate our constraints when manufactured within our tolerances. The Monte Carlo simulation used earlier is also used to evaluate the constraints for a sample of mechanisms. The results confirm that the original, or unadjusted, constraints are not violated.

2.3 Concluding Remarks

In this chapter we have presented a new geometric model for use in design optimization of constant-force compliant mechanisms. This model provides more freedom for the optimization than the model used in previous work by giving individual nodes complete freedom to relocate within the design domain. The implementation of this model resulted in a significant increase in percentage of constant force. Using the previous model a deterministic design was found with a 73.20% constant force, a value that we increased to 97.50% by using the new model.

This chapter also presented manufacturing uncertainties that may be encountered when producing constant-force compliant mechanisms, and explored specific situations that may alter the mating condition of the mechanism parts. To control these situations we developed a nondeterministic model of the mechanism, and formulated a design optimization problem that not only reduced the variation in performance, but increased the performance even more (98.20%). This was made possible by allowing the optimizer to design gaps and interference fits.

Table 2.3: Comparison of the Numerical Results

Design	C	$\bar{C}$	s_c
Benchmark	73.20%	70.24%	1.68%
Deterministic	97.50%	94.82%	2.46%
Non-deterministic	98.20%	97.64%	0.76%

A Monte Carlo simulation has verified that the non-deterministic design performed as expected. The average percentage constant force for the non-deterministic design is 97.64% with a standard deviation of 0.76%. This can be compared to the Monte Carlo results from the deterministic optimization, 94.82% constant with a standard deviation of 2.46%. Table 2.3 gives a summary of the comparison between these three designs.

Chapter 3

Surrogate Modeling Approach

This chapter presents an approach to robust optimization of constant-force mechanisms using surrogate modeling methods, following the procedure given in [3]. Essentially we create a polynomial, using statistical methods, to replace the finite element analysis during the optimization routine. This strategy allows us to efficiently explore more of the design space within the tolerance window to characterize sensitivity. It is limited by the number of factors we can include in the model, and how well the model fits the data. A review of the finite element method and optimization is included first, after which a procedure for the surrogate model approach is given. The process is demonstrated by an example. As in Chapter 2 only circular cams are used for convenience.

3.1 Model and Optimization Development

This section reviews the methods used in the last chapter to design a constant force mechanism. The first part of this section reviews the finite element model, and the second reviews the optimization routine. The material in both sections is used when building and optimizing the surrogate model that we use later in section 3.2.

3.1.1 Finite Element Model

Figure 3.1 illustrates the finite element model we use for a constant-force compliant mechanism. As shown in the figure, the multiple bend spring member is defined in the model by two dimensional beam elements and nodes. Each node is located using Cartesian coordinates (x and y). One end of the spring has fixed boundary conditions, and one node (at the point of contact) has an applied displacement (Δ) to which there is a reaction force

(F). The end opposite of the fixed end makes contact with the cam. The cam is defined by a center point with x and y coordinates, and a radius (r_c).

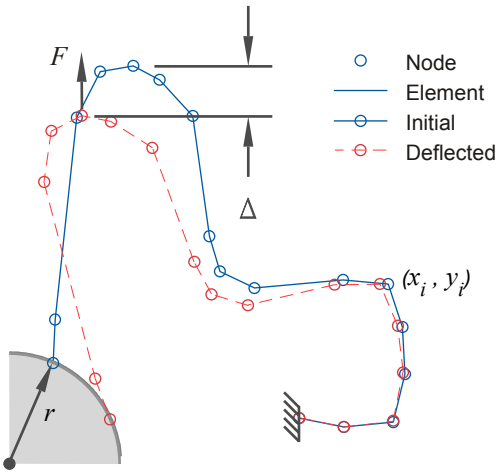

Figure 3.1: Finite element model of a constant force compliant.

This cam represents a contact target surface in the finite element code. Since mating uncertainty is considered, the finite element code must allow various mating conditions. The three principle conditions we must allow are a gap, interference, or contact. With a gap the end of the spring is allowed to move freely until it makes contact at which point it must follow the cam profile. With an interference we must first allow the interference to deform the spring, since this is what will happen during assembly. This will remove the initial interference and the spring will then have an initial stress and deformation condition. When we now apply the deflection load (Δ) we must be certain that it represents the net deflection (assembly deflection, preload, and operating load) of the node at which it is applied, so that the final position of the node will be the same regardless of the initial mating condition. Which mating condition we have depends entirely on the coordinates of the final node in the spring, the coordinates of the cam center, and the cam radius.

When applying the deflection (Δ) to the spring we divide it in many smaller substeps. We do this to both help the analysis converge on a solution, and to help build a force-deflection curve. At each substep we can determine the reaction force (F) which represents the force we want to hold constant. We can then plot the force-deflection curve

of the mechanism as shown in Figure 3.2. As seen in the figure for a small range of deflections the force rises quickly, after which the force remains nearly constant for a large displacement range. This is the range we want to operate in, and so a preload is applied to the mechanism. Within the operational displacement range the force does vary slightly resulting in a maximum force at some displacement and a minimum force at another. If these two forces were the same magnitude the force would be perfectly constant. The ratio of these forces, ranging from zero to one, is used to determine a constant force percentage for the mechanism.

$$C = 100\frac{F_{min}}{F_{max}} \tag{3.1}$$

This value and the parameters defined in the finite element model become the objective and the design variables in the optimization routine that is defined in the next part of this section.

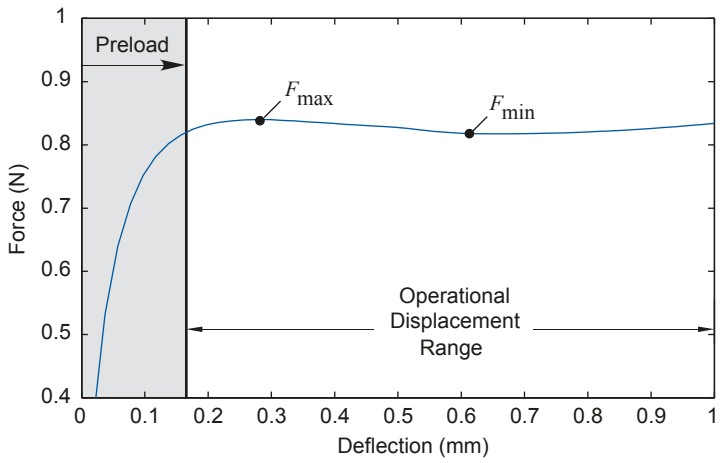

Figure 3.2: A typical force-deflection curve for a constant force mechanism.

3.1.2 Optimization Formulation

Here we define an optimization routine that will design constant force mechanisms. As presented in this section the optimization is done using deterministic values. In reality all of the design variables, and parameters are uncertain, and so the objective and each of the constraint values will also be uncertain. Section (3.2) will discuss the modifications we

make for uncertainty.

$$\max_{v} C(v,p) \tag{3.2}$$

subject to

$$0 \leq x_i \leq B_1 \qquad (i = 1,2,...,n-1) \tag{3.3}$$

$$0 \leq y_i \leq B_2 \qquad (i = 1,2,...,n-1) \tag{3.4}$$

$$d_{ij} > B_3 \qquad (i,j = 1,2,...,e, j > i+1) \tag{3.5}$$

$$\alpha_i \geq B_4 \qquad (i = 1,2,...,e-1) \tag{3.6}$$

$$L_i \geq B_5 \qquad (i = 1,2,...,e) \tag{3.7}$$

$$R_i \geq r_c \qquad (i = 1,2,...,n) \tag{3.8}$$

$$B_6 \geq \theta_c \geq B_7 \tag{3.9}$$

$$\gamma_0 \leq B_8 \tag{3.10}$$

$$\gamma_d \geq B_9 \tag{3.11}$$

$$F_{\max} \leq B_{10} \tag{3.12}$$

$$F_{\min} \geq B_{11} \tag{3.13}$$

$$\sigma_{\max} \leq B_{12} \tag{3.14}$$

where p is a set of designer defined design parameters listed in Table 3.1, and v is a set of design variables consisting of x and y coordinates, as well as r_c. B is a set of constraint limits for the constraints as outlined in Chapter 2. The constrained values are shown in Figure 3.3. Equations 3.3 and 3.4 constrain the nodes to remain within a two dimensional space B_1 wide and B_2 high. This constraint does not however apply to the center of the cam which is free to move anywhere. Equation 3.5 constrains the minimum distance between two elements (d_{ij}) so that no two elements cross over each other. Equations 3.6 and 3.7 constraint the smallest angle and the smallest length that is allowed for a bend in the spring. This ensures that the design is manufacturable. Equation 3.8 constrains how close

Table 3.1: Parameter Description for Deterministic Optimization

Parameter	Description
x_o	x Coordinate of Fixed Point
y_o	y Coordinate of Fixed Point
x_a	x Coordinate of point where force is applied
y_a	y Coordinate of point where force is applied
E	Young's Modulus
ν	Poisson's Ratio
w	Cross section width
h	Cross section height

each node can get to the cam center to keep the optimizer from placing nodes inside the cam. We only want to use the a portion of the cam that we are going to manufacture, thus Equation 3.9 restricts the part of the cam that will be used. We also place restrictions on the transmission angle (γ) both before deflection (γ_0) and after (γ_d). The transmission angle γ must initially be less than π because this is a kinematic change point. After deflection, the transmission angle γ_d must be greater than $\pi/2$ because a smaller angle will result in the element running through the cam. These constraints are given in Equations 3.10 and 3.11. Equations 3.12 and 3.13 keep the reaction force within a desirable range, and Equation 3.14 keeps the spring from yielding.

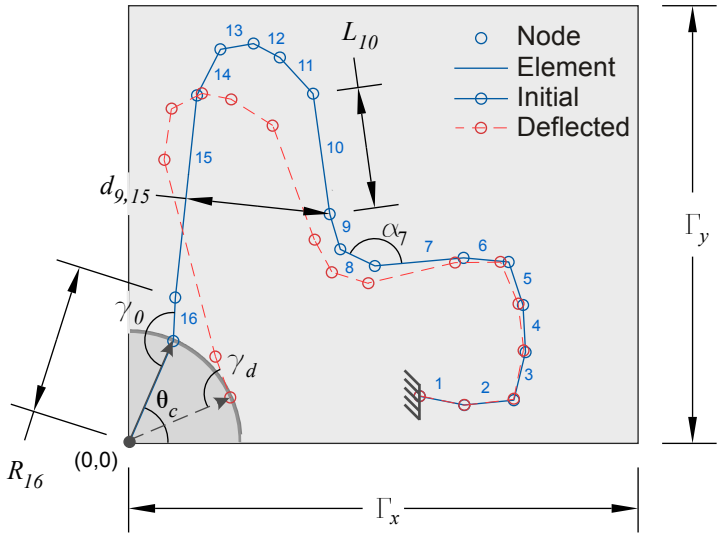

Figure 3.3: Values that are constrained during the optimization.

As mentioned before the evaluation of the objective depends on the results of the finite element analysis. Several constraints are also dependent on the finite element analysis (Equations 3.11-3.14) because we must know what the deflected shape, internal stresses, and reaction forces are before we can evaluate these constraints. This means that when we build a surrogate model for the objective value we must also build one for these constraints.

3.2 Surrogate Modeling Process

We now want to consider uncertainty in our mechanism model. Each of the parameters listed in Table 3.1 is subject to uncertainty as well as each of the design variables. For each uncertain value there is a known tolerance range, and the value is assumed to be normally distributed about the nominal value. The design approach will focus on finding a design that consistently performs well when the uncertain values are within the tolerance range. To verify the results a Monte Carlo simulation is used.

The subsections below outline the procedure for the design process. In the next section this procedure is applied using the example from Chapter 2.

3.2.1 Select a Starting Design

The first step in this procedure is selecting a starting point for the variable values. We would like to select a starting design that is feasible and somewhere near the optimum. This will help the optimization converge on a solution faster, and may avoid difficulties in finding a feasible solution. This is especially important since some of the constraints are being approximated by a surrogate model. This is done by first optimizing the mechanism using the deterministic optimization developed earlier.

3.2.2 Run a Screening Experiment

In most cases there are too many design variables and parameters to build an accurate surrogate model that includes them all. For each node in the finite element model there are two variables (x and y), the design variables also include the coordinates of the cam center, the radius of the cam, the cross sectional dimensions of the compliant member, and

the material properties of the spring. If the number of nodes in our finite element model is reduced the number of variables is also reduced, but there are fewer degrees of freedom for the optimizer.

A screening experiment is one solution to this problem. The screening experiment is only run once, and can therefore include more variables than the experiments within the optimization routine. Since a nodal location depends on two variables it is likely that second order interactions between design variables have a significant effect on the response of the finite element analysis, and since the finite element analysis is nonlinear it is likely that a nonlinear model is needed to fit the data from the experiment. Because a Box Behnken design is capable of keeping second order interactions from being confounded with each other, and capable of producing nonlinear models, it is a suitable for sampling the tolerance region surrounding the starting design.

After sampling the the tolerance region we must build a screening model to find the most significant factors in the performance. Linear regression is used to fit a second order polynomial including second order interactions. The equation for this model is given below.

$$\hat{C} = k_0 + \sum_{i=1}^{m} k_i U_i + \sum_{i=1}^{m} \sum_{j=i+1}^{m} k_{ij} U_i U_j + \sum_{i=1}^{m} k_{ii} U_i^2 \tag{3.15}$$

Each term in the model has a coefficient (k) that determines how significant the term is in the overall prediction of performance. By comparing these terms we can identify which uncertain values should be used to build the surrogate model for the optimization. As will be shown in Section 3.3 the most significant factors for the example design are the coordinates for the cam center, the coordinates for the point that makes contact with the cam, and the cam radius. Note that these are all of the factors that determine our mating condition. These five factors are therefore chosen to build a surrogate model.

3.2.3 Build a Surrogate Model

Now that the most significant factors have been identified, we must build a surrogate model for the optimization objective function and constraints. In many ways this is similar to building the screening model. The first step is selecting a sampling strategy. Because

there are only five factors and we still expect nonlinear behavior, a 3^5 full factorial sampling strategy is appropriate.

With more samples we can now model higher order interactions. Linear regression is again used, but with the model shown in the equation below.

$$\begin{aligned}\hat{C} = k_0 + \sum_{d=1}^{m} k_d u_d + \sum_{d=1}^{m}\sum_{f=d+1}^{m} k_{df} u_d u_f + \sum_{d=1}^{m}\sum_{f=d+1}^{m}\sum_{g=f+1}^{m} k_{dfg} u_d u_f u_g + \\ \sum_{d=1}^{m}\sum_{f=d+1}^{m}\sum_{g=f+1}^{m}\sum_{i=g+1}^{m} k_{dfgi} u_d u_f u_g u_i + \\ \sum_{d=1}^{m}\sum_{f=d+1}^{m}\sum_{g=f+1}^{m}\sum_{i=g+1}^{m}\sum_{j=i+1}^{m} k_{dfgij} u_d u_f u_g u_i u_j + \sum_{d=1}^{m} k_{dd} u_d^2\end{aligned} \tag{3.16}$$

This model equation includes all linear terms and squared terms for each variable, as well as all possible combinations of interactions between the variables. When the screening model was built the manufacturing tolerance limits defined the trust region. In the optimization model its necessary to explore the region beyond the tolerance limits. We therefore use a larger trust region, but decrease the size of the trust region after each complete optimization search. This moves the search quickly to an area near the optimum, and then searches that area with increasing accuracy.

3.2.4 Build Constraint Models

We mentioned earlier the need to create surrogate models for the constraint values as well as the objective value. This is because Equations 3.11-3.14 cannot be evaluated without the results of the nonlinear finite element analysis. Since the finite element analysis is used to build the objective surrogate model we can also build constraint surrogate models at the same time using the same analysis.

Because the constrained values depend on the uncertain variables and parameters it is necessary to ensure that the constraints are robust, meaning they will not be violated by variations within the tolerance range. For the values that are independent of the finite element analysis we can determine the extremes of the constrained values that the tolerances will allow and shift the B constants by that amount. For those dependent on the finite element analysis the surrogate model can now be used to determine the extremes and those B

constants can also be shifted. Because some constraints are now evaluated using surrogate models we must verify that the original constraints are not violated in the final design. The Monte Carlo simulation can do this.

3.2.5 Optimize and Iterate

The optimization formulation for the surrogate model approach is shown below.

$$\max_{u} J = W_1\hat{C} + W_2\frac{\hat{C}_{min}}{\hat{C}_{max}} \tag{3.17}$$

subject to

$$0 \leq x_i \leq \tilde{B}_1 \qquad (i = 1,2,...,n-1) \tag{3.18}$$

$$0 \leq y_i \leq \tilde{B}_2 \qquad (i = 1,2,...,n-1) \tag{3.19}$$

$$d_{ij} > \tilde{B}_3 \qquad (i,j = 1,2,...,e, j > i+1) \tag{3.20}$$

$$\alpha_i \geq \tilde{B}_4 \qquad (i = 1,2,...,e-1) \tag{3.21}$$

$$L_i \geq \tilde{B}_5 \qquad (i = 1,2,...,e) \tag{3.22}$$

$$R_i \geq \tilde{r}_c \qquad (i = 1,2,...,n) \tag{3.23}$$

$$\tilde{B}_6 \geq \theta \geq \tilde{B}_7 \tag{3.24}$$

$$\gamma_0 \leq \tilde{B}_8 \tag{3.25}$$

$$\hat{\gamma}_d \geq \tilde{B}_9 \tag{3.26}$$

$$\hat{F}_{\max} \leq \tilde{B}_{10} \tag{3.27}$$

$$\hat{F}_{\min} \geq \tilde{B}_{11} \tag{3.28}$$

$$\hat{\sigma}_{\max} \leq \tilde{B}_{12} \tag{3.29}$$

where $\hat{C}_{min}$ and $\hat{C}_{max}$ are the minimum and maximum approximations of C within our tolerance window that we sample. This value is similar to the ratio defined in Equation 3.1,

only this is a percentage of variation of the approximation ($\hat{C}$) within the tolerance window. The tilde in the constraint equations designates values that have been shifted to account for uncertainty, and the hat designates values that have been approximated by surrogate models. In the aggregate objective function W_1 and W_2 are the weighing factors.

The remainder of the procedure involves simply iterating these steps. After each iteration we decrease the trust region as explained earlier, then rebuild the surrogate models using our latest solution as the starting design for building the model. The iterations end when our trust region is the same size as our tolerance region, and we have reached a suitable optimum.

3.3 Example and Results

In this section we use the procedure outlined above to solve a specific design problem. The parameters of the problem are given in Table 3.2.

Table 3.2: Parameters Used for the Example Problem

Parameter	Description	Value
x_o	x Coordinate of Fixed Point	4.04 mm
y_o	y Coordinate of Fixed Point	0.51 mm
x_a	x Coordinate of point where force is applied	1.54 mm
y_a	y Coordinate of point where force is applied	5.81 mm
E	Young's Modulus	110 GPa
ν	Poisson's Ratio	0.34
w	Cross section width	1.00 mm
h	Cross section height	0.2 mm

We use the deterministic optimization to find a suitable starting design with these parameters. The starting design is 97.5% constant, and a Monte Carlo simulation shows that the standard deviation is 2.46%. This is the deterministic solution we found in Chapter 2.

The next step in the procedure is to make a screening model. We use the coefficients of each term (k_i) to rate its significance in the model. Below is a Pareto chart of the thirty most significant coefficients ordered by decreasing significance. Note that there is a drop in

magnitude after the twentieth coefficient. When we examine the top twenty coefficients we find that they correspond to linear terms, squared terms, and all possible combinations of interaction terms for the five variables that determine the mating condition (the coordinates for the cam center, the coordinates for the node the mates with the cam, and the cam radius). Based on this evidence we choose these variables to build our optimization surrogate model.

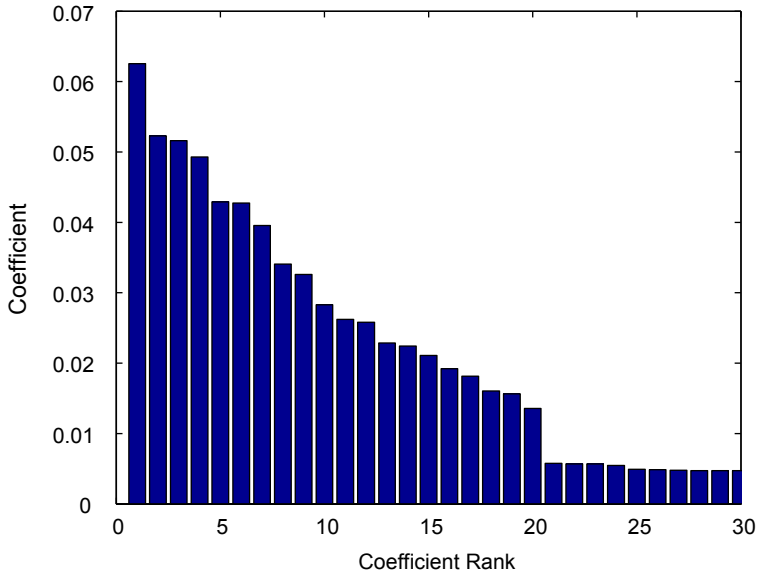

Figure 3.4: Pareto chart showing the thirty most significant coefficients.

When we build the optimization model we use a trust region of three times the tolerance limits to start with. At each iteration we decrease the value by 10%. This increases the accuracy of our model as the design process continues. At the end of the process we have an R^2 value of 94.71%, suggesting that the model fits the data fairly well. With this model we find an optimum that is suitable as shown in Figure 3.5. This final design is 93.61% constant when analyzed with the original finite element method. This performance value is lower than the starting design, but that is not surprising since we have added a new objective, and our optimization is based on an approximation of the finite element model.

The Monte Carlo simulation confirms the robustness of this design, as well as the robustness of the constraints. Figure 3.6 shows a histogram for the performance of the

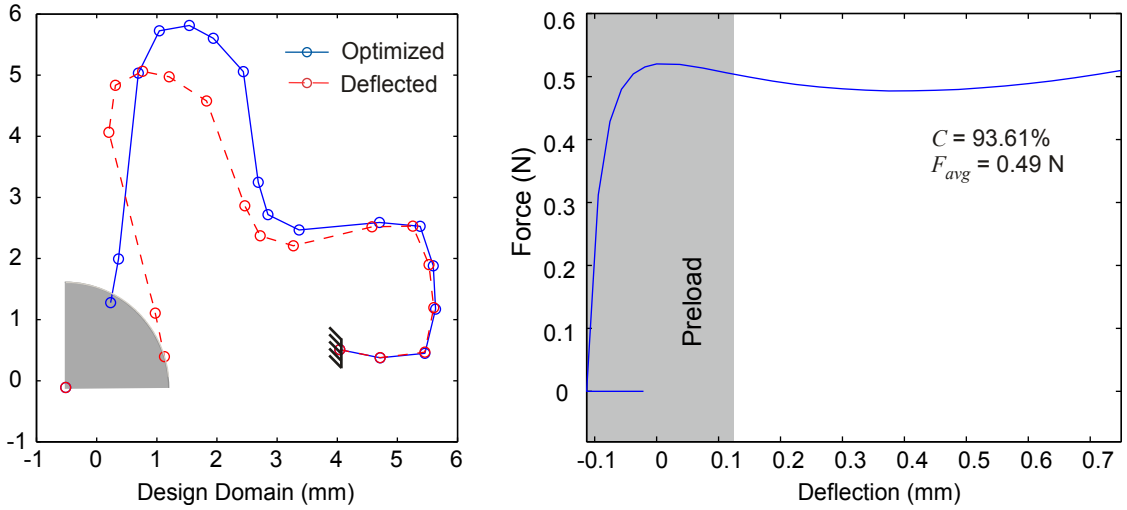

(a) (b)

Figure 3.5: The solution design from the surrogate model approach. (a) The initial and deflected positions of the design. (b) The force-deflection curve of the design.

solution design. We see that the new design has a smaller standard deviation of 0.77%, whereas the starting design had a standard deviation of 2.46%.

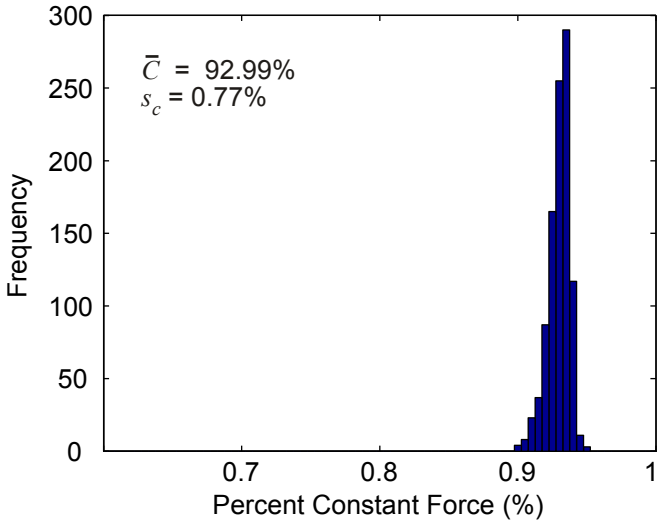

Figure 3.6: Histogram of the Monte Carlo results for the final design using 1,000 samples.

3.4 Conclusion

This chapter has taken the next step in the development of a design strategy for robust constant-force mechanisms. In the last chapter we only optimized sensitivity using three extreme mating conditions. To this method we have now added a surrogate model approach that allows us to more thoroughly explore the design space within the tolerance limits. In the example problem this results in a solution that is 93.61% constant with a standard deviation of 0.77%. This is less desirable than the optimal design found in Chapter 2 that was 97.50% constant with a standard deviation of 2.46%. This drop in performance is most likely caused by the inaccuracy introduced with the polynomial fit. The optimization routine uses only an approximation of the finite element method, which may result in a high value for $\hat{C}$ but a significantly lower value for C. Further refinement of the surrogate model can be done to better approximate the finite element method and achieve better results. The results of the screening experiment and optimization do, however, support the idea that we can successfully control the sensitivity of constant-force mechanism by optimizing the variables that control the mating condition.

Chapter 4

Frictional Sensitivity and Non-circular Cams

The last two chapters have focused on reducing sensitivity to manufacturing and mating uncertainties. The optimal designs were compared and evaluated using the standard deviation in performance from a Monte Carlo simulation. This chapter focuses on reducing the effect of friction while all input variables and parameters are considered deterministic thus, the optimal design does not necessarily have a lower standard deviation. The optimizer is expanded to allow the design of elliptical cams. This is done to further increase the design freedom. Again a review of the finite element model is provided, then a discussion of frictional effects is followed by an optimization formulation to reduce frictional sensitivity. We demonstrate the method with an example. [4]

4.1 Model Development

In this section we develop a model for estimating the force-deflection relationship of a compliant constant-force mechanism subject to frictional forces. We first present the finite element model, and then discuss the effect friction has on a compliant constant-force mechanism with a simulated pin joint. We also discuss the implementation of elliptical cams.

4.1.1 Finite Element Model

We use a nonlinear finite element method to model the constant-force compliant mechanism. In this model, as shown in Figure 4.1, the geometry of the compliant member is represented by a series of two dimensional frame elements each of which has six degrees of freedom for motion. Each node is defined by Cartesian coordinates (x_i, y_i) which are

used later as variables in the design optimization, with two exceptions. The first is an end node of the spring that has fixed boundary conditions, and whose position is predetermined. The second is a specified interface node where the input deflection (Δ) is applied in step intervals, whose position is also predetermined. At the free end of the compliant member is the cam. The finite element analysis uses an iterative approach to determine the internal stresses and reaction forces within the compliant member. The end result is a vector of reaction forces (F) for each displacement substep, which we use to define a force-deflection curve as shown in Figure 4.2.

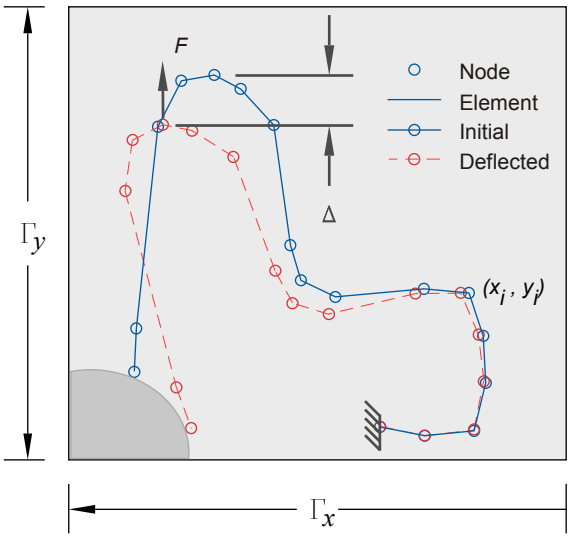

Figure 4.1: The finite element model for a constant-force compliant mechanism.

In this chapter we make our first exploration into using non-circular cams. Specifically we use a cam that can be defined by the equation for an ellipse:

$$r^2 = \frac{(y-y_c)^2}{a} + \frac{(x-x_c)^2}{b} \tag{4.1}$$

where r, a, b, x_c, and y_c are constants that become design variables in an optimization routine described shortly. Although we use an ellipse in this model for convenience, any arbitrary cam profile could be used. To model the cam in the finite element analysis we must use principles of contact mechanics. The free end of the compliant member can be in contact with the cam, interfere with the cam, or be separated from the cam by a gap.

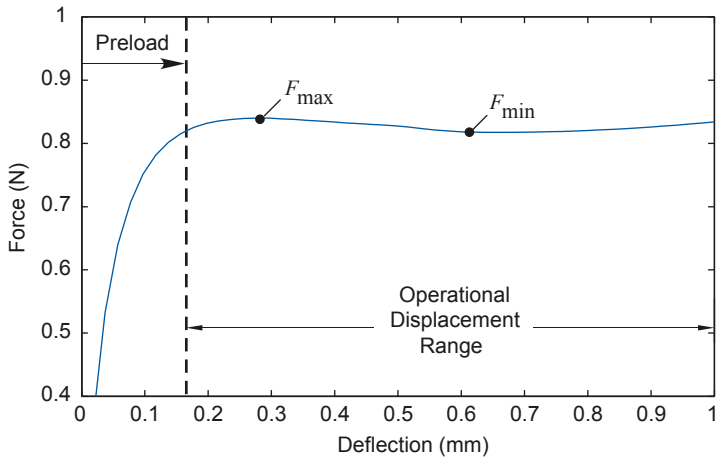

Figure 4.2: A typical force-deflection curve for a constant-force mechanism.

Interferences are handled by forcing the solution routine to remove the interference. When in contact the free end is constrained to follow the cam profile. We do this by using linear constraints with Lagrangian multipliers. By solving for the Lagrangian multipliers we can also determine the normal force applied to the end of the compliant member by the cam. We later use this normal force to determine frictional effects.

4.1.2 Frictional Effects

As discussed earlier, the interaction between the compliant member and the cam plays an important role in the constant force attribute of the simulated pin-joint mechanism, in that the force developing from the deflected member and the force transmitted to the deflected member from the cam interface are carefully balanced as shown in Figure 1.2(b). As the compliant member is compressed and makes contact with the cam a reaction force normal to the cam surface is created as shown in Figure 4.3. A portion of this normal force acts in the direction opposing the applied deflection and along with the internal forces of the compliant member creates the net output force which is maintained constant. The Coulomb friction between the cam and the compliant member also creates a force, but one that is tangent to the cam surface. A portion of this force also contributes to the net output force, but whether it adds to or subtracts from the output force depends on the direction of

motion at the cam interface. This results in variations in the force-deflection curve as seen in Figure 4.4(a)a.

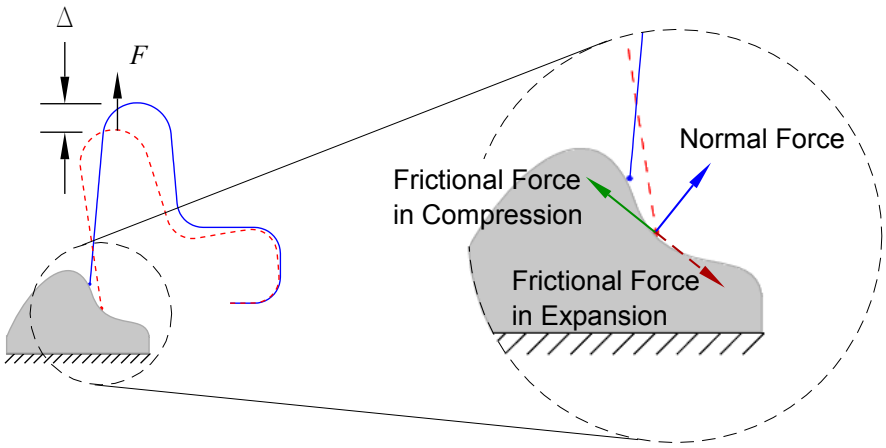

Figure 4.3: The interaction forces that develop at the cam interface as a deflection is applied to the mechanism.

The top curve in Figure 4.4(a) shows the force-deflection relationship as the applied deflection is increasing, or as the compliant member is being compressed. The bottom curve shows the force-deflection relationship as the applied deflection is decreasing, or as the compliant member is being expanded. The area between these curves (E_f) represents the energy that is lost by friction when the mechanism undergoes a fully reversed deflection in the operational range. As can be seen in the figure, a design that may exhibit good constant-force performance from a frictionless point of view can have a much worse performance if friction is present, especially if the motion varies between compression and expansion. An example of this situation is in the case of vibratory motion. In order to design a constant-force mechanism that will perform well under such conditions we must reduce the difference between the compression and expansion curves, which is equivalent to reducing the frictional energy loss if we use a constant deflection range. Figure 4.4(b) shows what the force-deflection curves might look like for a design that has minimized frictional energy loss. Importantly we note that we can exclude the energy losses within the preload deflection range, since the mechanism will not operate at these deflections after the

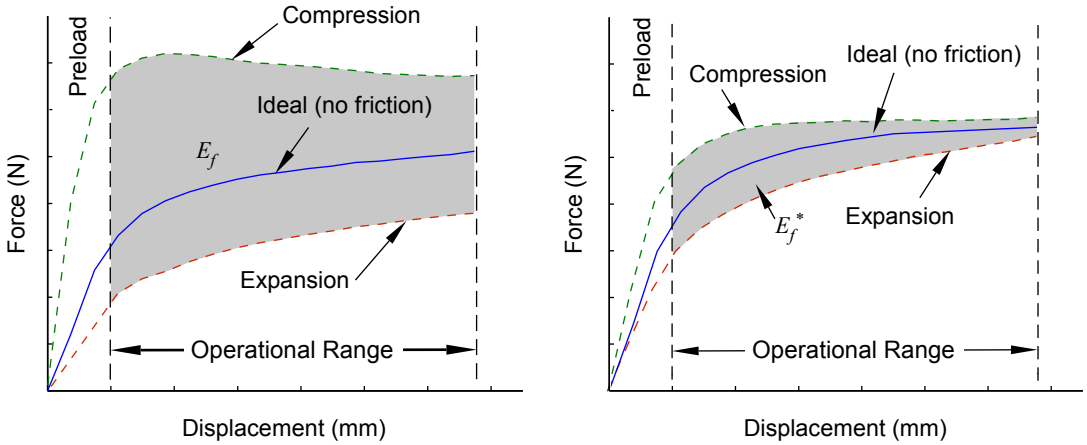

Figure 4.4: The force-deflection curve of a constant-force compliant mechanism with variations caused by friction. (a) The curves of an initial design with the energy loss (E_f). (b) The curves of an optimized design when energy loss has been minimized (E_f^*).

initial assembly. In order to minimize E_f we must first be able to calculate its magnitude using our finite element model.

The normal force that we calculate in the nonlinear finite element analysis from the Lagrangian multipliers is the normal force shown in Figure 4.3. Once this force is known we use Coulomb's theory of friction to make an estimate of the tangential friction force (F_f).

$$F_f = \mu N \tag{4.2}$$

where N is the normal force, and μ is the coefficient of friction. When using Equation 4.2 we assume that the coefficient of friction can be found experimentally, and that it remains constant as the design variables change. We can then apply the friction force to the free end of the compliant member in the direction opposite the motion, and iterate the finite element deflection calculations until we converge on a solution. This will give us the force-deflection relationships for the compression and expansion motions of the mechanism which we use to numerically calculate the energy loss (E_f).

4.2 Optimization Formulation

The finite element analysis gives us the information we need to construct the force-deflection curve as shown in Figure 4.2. As seen in the figure the reaction force cannot be held exactly constant over the operational displacement range and we get a maximum force (F_{max}) and a minimum force (F_{min}). We use these values to define the constant force percentage (C) for the mechanism.

$$C = 100\frac{F_{min}}{F_{max}} \tag{4.3}$$

We can now use a multi-objective design optimization approach to search for designs that have a high value of C while minimizing the energy loss due to friction (E_f). We formulate an aggregate objective (J) as a weighted sum of our two objectives. Our design optimization then becomes:

$$\min_{v} J = -W_1 C(v,p) + W_2 E_F(v,p) \tag{4.4}$$

subject to Equations 4.5-4.22 where W_1 and W_2 are weights, p is a vector of design constants, and v is a vector of design variables consisting of the x and y coordinates of each node in the compliant member, except the two fixed nodes as explained earlier, and the constants r, a, b, x_c, and y_c from Equation 4.1. Note that in previous chapters a circular cam was used which is equivalent to removing a and b from the design variables and keeping them equal. By allowing the optimization routine to choose different values for a and b we increase the feasible design space by including designs with elliptical cams also. Although we could use any arbitrary profile for the cam, we use an ellipse because the previous chapters have demonstrated the functionality of circular cams, which are a special case of elliptical cams.

We must define a feasible space using several constraints that represent our manufacturing limitations, as well as some limitations in our finite element model.

$$0 \leq x_i \leq \Gamma_x \qquad (i = 1,2,...,n) \tag{4.5}$$

$$0 \leq y_i \leq \Gamma_y \qquad (i = 1,2,...,n) \tag{4.6}$$

$$0 \leq r \leq r_{max} \tag{4.7}$$

$$0 \leq a \leq a_{max} \tag{4.8}$$

$$0 \leq b \leq b_{max} \tag{4.9}$$

$$x_{min} \leq x_c \leq x_{max} \tag{4.10}$$

$$y_{min} \leq y_c \leq y_{max} \tag{4.11}$$

$$d_{ij} > 0 \qquad (i,j = 1,2,...,e \quad j \neq i, j \neq i \pm 1) \tag{4.12}$$

$$\alpha_i \geq \alpha_{min} \qquad (i = 1,2,...,e-1) \tag{4.13}$$

$$L_i \geq L_{min} \qquad (i = 1,2,...,e) \tag{4.14}$$

$$\varepsilon_i \geq 0 \qquad (i = 1,2,...,n-1) \tag{4.15}$$

$$\varepsilon_{min} \leq \varepsilon_n \leq \varepsilon_{max} \tag{4.16}$$

$$\gamma_0 \leq \gamma_{max} \tag{4.17}$$

$$\gamma_d \geq \pi/2 \tag{4.18}$$

$$x_{nd} \geq x_c \tag{4.19}$$

$$y_{nd} \geq y_c \tag{4.20}$$

$$F_l \leq F \leq F_u \tag{4.21}$$

$$\sigma_{\max} \leq S_y/S_F \tag{4.22}$$

The first two constraints, Equations 4.5 and 4.6, set up a design domain that limits the physical space that our mechanism can occupy. Equations 4.7-4.11 place limits on the values that determine our cam profile. We keep the elements from crossing over each other by constraining the minimum distance between any two non-adjacent elements (d_{ij}) in Equation 4.12. Constraint Equations 4.13 and 4.14 keep the optimizer from creating bend

angles (α_i) or element lengths (L_i) that are too small to be manufactured. Equation 4.15 keeps any of the nodes from deflecting into the cam by constraining the minimum distance (ε_i) between the i-th node and the cam surface. Equation 4.16 is a special case of Equation 4.15 since the distance between the last node (ε_n) and the cam determines our initial contact condition. We allow the mechanism to be designed with an initial interference fit or a gap within the limits ε_{min} and ε_{max}. Some difficulties may occur if the axis of the final element and the direction of the normal force at the contact point are aligned. This is similar to a kinematic change point between two links. To avoid this we constrain the force transmission angle (γ_0) in Equation 4.17. At the fully deflected position we constrain this angle (γ_d) to be greater than $\pi/2$ which is the value of the angle if the deflected final element is tangent to the cam surface at the point of contact. If the angle is less than $\pi/2$ the final element will pass through the cam boundary. Equations 4.19 and 4.20 restrict the motion of the node at the free end in order to keep the deflected coordinates (x_n, y_n) in one quadrant of the ellipse equation. Finally we constrain the range of output reaction forces and the maximum bending stress in Equations 4.21 and 4.22 respectively.

4.3 Example and Results

We now illustrate this design method with an example. We use the example from previous chapters in which we design a constant-force contact that will be attached to a circuit board at coordinates (4.04, 0.51), and make contact with a mating device at coordinates (1.54, 5.81). The operational displacement range is 0.1125 mm to 0.75 mm. The constraint limits are listed in Table 4.1. We use as a starting design the mechanism we identified in Chapter 2 that is 98.20% constant when analyzed without considering friction. The first column in Table 4.2 lists the initial values for the design variables, material properties, and cross sectional dimensions. When we include frictional effects we find that the force-deflection curve in compression, and the curve in expansion enclose an area of 0.61 mJ, or in other words 0.61 mJ are lost from the frictional effects within the operational diplacement range. This results in a difference in output force as large as 1.73 N between the two motions. The force-deflection curve, and finite element model are shown in Figure 4.5 where the points with the maximum difference in force are shown as f_1 and f_2. As seen

Table 4.1: Constraint Limits for the Optimization.

$\Gamma_x\ (mm)$	12
$\Gamma_y\ (mm)$	6
$r_{max}\ (mm)$	6
a_{max}	2
b_{max}	2
$x_{min}\ (mm)$	-12
$x_{max}\ (mm)$	0.5
$y_{min}\ (mm)$	-6
$y_{max}\ (mm)$	5
$\alpha_{min}\ (deg)$	100
$L_{min}\ (mm)$	0.3
$\varepsilon_{min}\ (mm)$	-0.375
$\varepsilon_{max}\ (mm)$	0.375
$\gamma_{max}\ (deg)$	175
$F_l\ (N)$	0.3
$F_u\ (N)$	0.9
S_F	1

in the figure, the starting mechanism is designed to have an initial interference fit between the compliant member and the cam. This means that when the mechanism is assembled the compliant member will deflect slightly. In this case the assembly deflection is opposite the prescribed deflection (Δ) and a larger preload is required to reach the operational deflection range.

We now perform the optimization search as defined earlier to maximize the constant force percentage, while reducing the difference in our output force during the compression and expansion strokes by reducing the energy loss. In this example we use equal weights on both objectives. Figure 4.6 shows the optimal force-deflection curve and finite element model, and the second column in Table 4.2 lists the optimal variable values. As can be seen in Figure 4.6 the energy loss from friction has been reduced by approximately 36%, from 0.61 mJ to 0.39 mJ, and the maximum difference in output force (between points f_1^* and f_2^*) has been reduced to 0.77 N. This is accompanied, however by a loss in constant-force percentage (C) from 98.20% to 79.57%. This is not unexpected since there are two objectives that may compete with each other. We also note that the optimal values for a and b are unequal, making the cam slightly elliptical, and that the final element is again

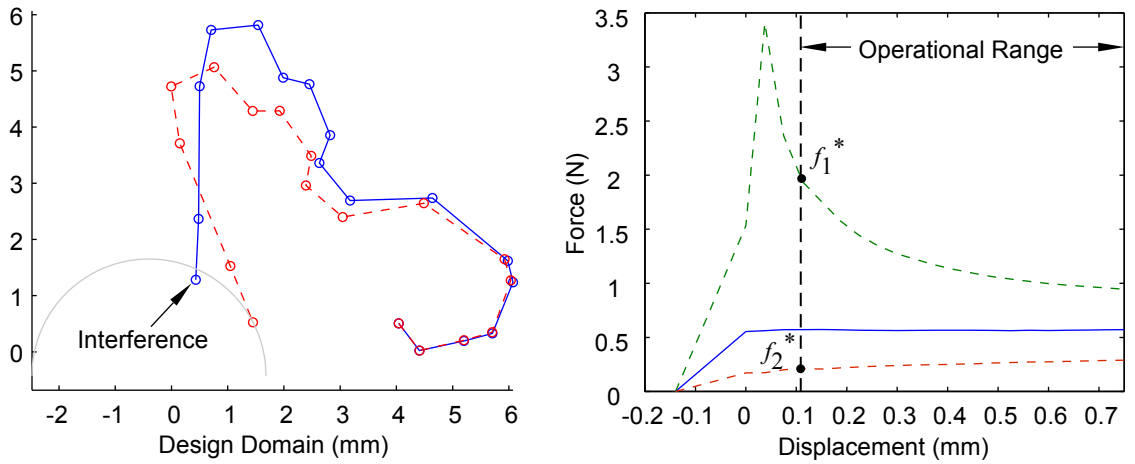

(a) (b)

Figure 4.5: Starting design for the optimization with 98.20% constant force and 0.61 mJ loss to friction. (a) The design domain with the starting geometry. (b) The force-deflection curves for the design.

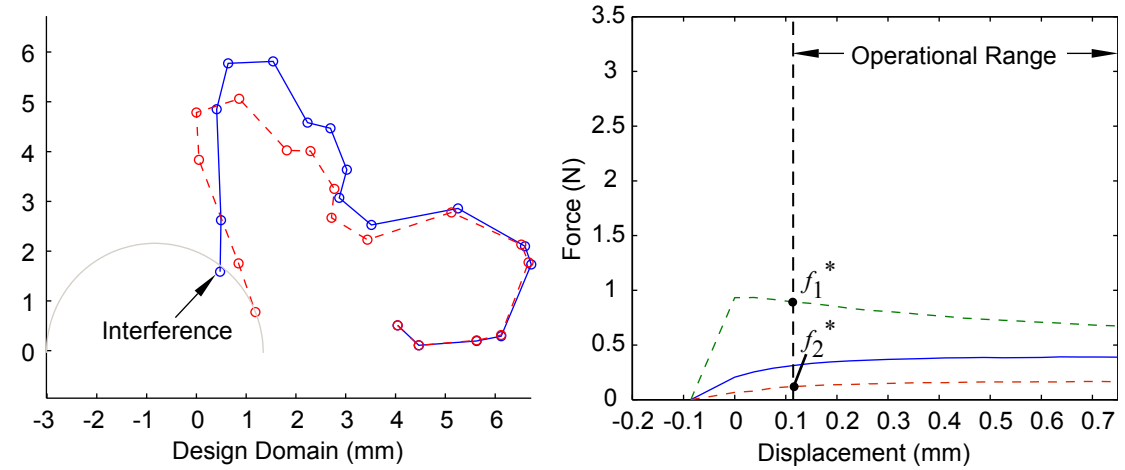

(a) (b)

Figure 4.6: Optimal design with 79.57% constant force and 0.39 mJ loss to friction. (a) The design domain with the optimal geometry. (b) The force-deflection curves for the design.

Table 4.2: Design Variables and Constants for the Initial and the Optimized Designs.

x y coordinates (mm)	Starting Design		Optimal Design	
	x	y	x	y
	4.04	0.51	4.04	0.51
	4.41	0.02	4.47	0.11
	5.20	0.20	5.63	0.19
	5.71	0.33	6.12	0.29
	6.07	1.24	6.73	1.73
	5.98	1.62	6.60	2.10
	4.64	2.74	5.26	2.86
	3.18	2.69	3.51	2.53
	2.63	3.36	2.87	3.07
	2.82	3.86	3.02	3.63
	2.45	4.76	2.69	4.47
	1.99	4.88	2.23	4.58
	1.54	5.81	1.54	5.81
	0.71	5.73	0.64	5.77
	0.50	4.73	0.41	4.85
	0.48	2.37	0.49	2.62
	0.43	1.28	0.48	1.59
x_c (mm)	-0.40		-0.83	
y_c (mm)	-0.43		-0.05	
r (mm)	2.08		2.28	
a	1.00		0.94	
b	1.00		0.91	
Modulus (MPa)	110.0E+3		110.0E+3	
Poisson ratio	0.34		0.34	
μ	0.50		0.50	
S_y (MPa)	552		552	
w (mm)	1.00		1.00	
h (mm)	0.20		0.20	

designed to interfere with the cam during assembly. This example demonstrates our method of identifying a constant-force compliant mechanism whose performance is less affected by friction.

4.4 Conclusion

The design optimization we have presented in the preceding sections of this chapter can be used to minimize the negative effects of friction in the simulated pin joints of

some constant-force mechanisms. In the example of Section 4.3 we can find a reduction of approximately 36%. This can represent significant improvement in the performance of a mechanism that undergoes changing displacements. It is important to note that this reduction in frictional energy loss results from changing the shape of the mechanism and not the material or surface condition. In other words, we optimize the normal force (N) and not the friction coefficient (μ) in Equation 4.2 to achieve our desired performance. We also note that the optimized shape in our example required the use of an elliptical cam. This supports the idea that non-circular cams may be beneficial to the performance of constant-force mechanisms with simulated pin joints.

Chapter 5

Conclusions

5.1 Conclusions and Key Observations

This thesis has presented methods for improving the performance of cam-based constant-force compliant mechanisms, and demostrated the efficacy of these methods with examples from the design of electrical contacts. Table 5.1 shows the results from the examples in all of the preceding chapters. In this table, the key performance parameters are shown for each design. These parameters include: the constant-force percentage as evaluated by the finite element method, the standard deviation in constant-force percentage as evaluated by the Monte Carlo simulation, and the frictional energy loss. Some values are shown as N/A since the frictional energy loss and the standard deviation have not been evaluated for every design. These results show that both methods for reducing the standard deviation in performance are effective, and that the method for reducing frictional sensitivity is also effective. All of the designs have a higher constant-force percentage than the benchmark design. Based on the results, some general conclusions can be made about the design of constant-force mechanisms. These conclusions are given in the following sections.

Table 5.1: Comparison of the Various Mechanism Designs

Method of Design	C	s_c	E_f (mJ)
Benchmark Design	73.20%	1.68%	N/A
Deterministic Optimization	97.50%	2.46%	N/A
Mating Condition Optimization	98.20%	0.76%	0.61
Surrogate Optimization	93.61%	0.77%	N/A
Frictional Optimization	79.57%	N/A	0.39

5.1.1 The Role of the Cam Interaction

In each of the examples, the profile of the optimal design is similar to the profile of the initial design. Significant changes, however, occur in the cam location and the cam sizing. The screening experiment in the surrogate model approach identifies the variables defining the cam as the most significant variables in the performance estimation. This shows that, given a feasible starting design, improvement in performance is obtained primarily by optimizing the cam size and location. The optimal designs also make use of an initial interference between the compliant member and the cam. The benefit of designing a mechanism to have an interference fit is intuitive considering that an interference fit essentially increases the preload, and so the performance is evaluated on a smaller percentage of the entire deflection.

Based on these observations further research is recommended to better understand the influence of the cam interaction on performance. This thesis explores the use of circular and elliptical cams, while pointing out that any arbitrary shape could be used. Some cam profiles may be better suited for constant-force mechanisms and should be researched. Additionally some better performing spring profiles may be identified by considering new starting designs. One method of including several starting designs would be using a genetic algorithm for optimization.

5.1.2 Applications to Multiple Configurations

This thesis explores the use of only one configuration of the compliant constant-force mechanism (class 1A as defined by Howell [8]). A more thorough approach could be developed to find a set of solutions including several different configurations. One example might be the design shown in Figure 5.1 (class 3A as defined by Howell [8]). This configuration is a different class of mechanism still based on the slider-crank design, but this one replaces the pin joints with small-length compliant segments. This is similar to replacing the pin joints with a cam surface as was done throughout this thesis. In this configuration, however, there are no mating parts, which eliminates some of the key uncertainties that were presented in the previous chapters. While the formulations presented in this thesis

are made specifically for a cam-based design, they could be generalized to include this and other configurations. This may require developing new constraints or adjusting the constraints used in the examples of this thesis. The contact mechanics and frictional analysis included in the finite element method may not be applicable to every configuration (such as the one in Figure 5.1) while other analyses may be necessary to determine the force-deflection relationship using a finite element method. The objective functions used in this thesis, however, could be applied directly to nearly any constant-force mechanism configuration. This more general approach would give the designer a number of possibilities to choose from, which would be a significant help in the design of a system.

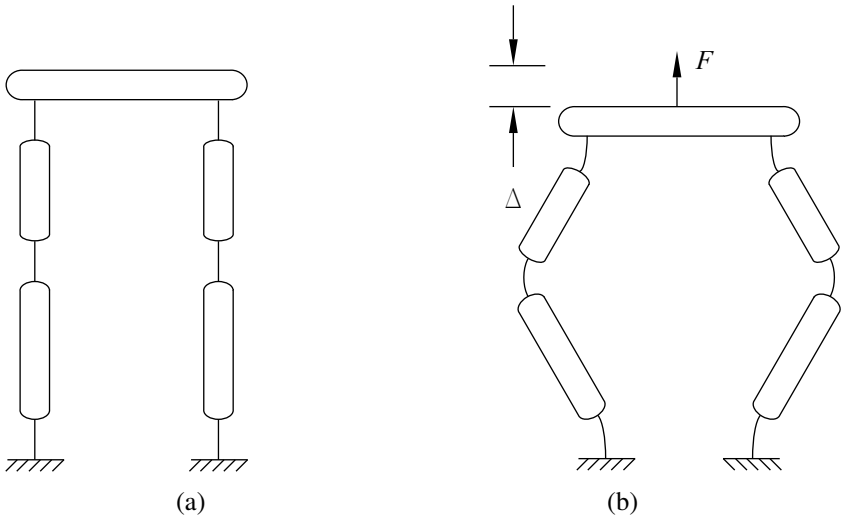

Figure 5.1: A different topology of a constant-force compliant mechanism. (a) The mechanism in its undeflected state. (b) The mechanism with an applied deflection (Δ)

5.1.3 Competing Objectives

Further conclusions regarding the design of cam-based constant-force mechanisms can be derived from the results of the frictional optimization. In this case, the optimizer reduced frictional sensitivity significantly, but at the cost of constant-force percentage. The results suggest that the two objectives (constant-force percentage and frictional sensitivity) are competing. This may be explained by recognizing that both the constant-force percent-

age and the frictional force are related to the normal force developed at the cam interface. The relation of the frictional force to the normal force is given by Coulomb's theory of friction, Equation 4.2. The constant-force percentage depends on this normal force since it is a part of the changing force transmitted from the cam to the compliant member, as was shown in Figure 1.2(b).

In this thesis robustness and frictional sensitivity are considered separately. It may be desirable to include both of these objectives and the constant-force percentage in one optimization. A better understanding of the relationship between these objectives could be reached, and by adjusting the weight factors in the aggregate objective function, or by experimenting with different types of aggregate objective functions, a Pareto front in the design space could be generated and evaluated.

References

[1] Weight, B. L., Mattson, C. A., Magleby, S. P., and Howell, L. L., 2007. "Configuration selection, modeling, and preliminary testing is support of constant force electrical connectors." *ASME Journal of Electronic Packaging,* **129**, pp. 236–246. xii, 4, 5, 6, 7, 8, 12, 20, 21

[2] Meaders, J. C., and Mattson, C. A., 2007. "Robust design optimization of compliant constant force contacts with simulated pin joints." No. AIAA 2007-1911, Proceedings of the AIAA/ASME/ASCE/AHS/ASC Structures, Structural Dynamics, and Materials Conference. 2, 8, 11

[3] Meaders, J. C., and Mattson, C. A., 2008. "Robust design optimization of a constant force mechanism using a surrogate modeling approach." No. AIAA-2008-900, Proceedings of the AIAA Aerospace Sciences Meeting and Exhibit. 2, 8, 27

[4] Meaders, J. C., and Mattson, C. A., 2008. "Minimization of frictional effects in simulated pin joints of constant-force compliant mechanisms." No. AIAA 2008-2063, Proceedings of the AIAA/ASME/ASCE/AHS/ASC Structures, Structural Dynamics, and Materials Conference. 2, 8, 41

[5] Meaders, J. C., and Mattson, C. A., 2008. "Design optimization to reduce sensitivity in constant-force contacts subject to mating uncertainty." *Journal of Structural and Multidisciplinary Optimization* [under revision]. 2

[6] Nahar, D. R., and Sugar, T., 2003. "Compliant constant-force mechanism with a variable output for micro/macro applications." Vol. 1, Proceedings of IEEE International Conference on Robotics and Automation, pp. 318–323. 2, 6

[7] Evans, M. S., and Howell, L. L., 1999. "Constant-force end-effector mechanism." Proceedings of the IEEE International Conference on Robotics and Applications, pp. 250–256. 2, 6

[8] Howell, L. L., 2001. *Compliant Mechanisms*. John Wiley & Sons, New York, NY. 2, 6, 7, 54

[9] Nathan, R. H., 1985. "A constant force generation mechanism." *ASME Journal of Mechanisms, Transmissions, and Automation in Design,* **107**, pp. 508–512. 5

[10] Bossert, D., Ly, U. L., and Vagners, J., 1996. "Experimental evaluation of a hybrid position and force surface following algorithm for unknown surfaces." Vol. 3, Proceedings of the IEEE International Conference on Robotics and Automation, pp. 2252–2257. 5

[11] Herder, J. L., and van den Berg, F. P. A., 2000. "Two spatially balanced compliant mechanisms (sbcm's), an example and prospectus." No. DETC-2000-MECH-14120, Proceedings of the ASME Design Engineering Technical Conferences. 5

[12] Jenuwine, J. G., and Midha, A., 1994. "Synthesis of single-input and multiple-output port mechanisms with springs for specified energy absorption." *ASME Journal of Mechanical Design,* **116**(3), pp. 937–943. 5

[13] Weight, B. L., 2001. "Development and design of constant-force mechanisms." Master's thesis, Department of Mechanical Engineering, Brigham Young University, Provo, UT. 6, 7

[14] Howell, L. L., and Magleby, S. P., June 13, 2006. Substantially constant-force exercise machine Patent No. US 7,060,012 B2. 6

[15] Murphy, M. D., Midha, A., and Howell, L., 1996. "The topological synthesis of compliant mechanisms." *Mechanism and Machine Theory,* **31**(2), pp. 185–199. 7

[16] Weight, B. L., Magleby, S. P., and Howell, L. L., 2002. "Selection of compliant constant-force mechanisms based on stress and force criteria." No. DETC-2002-MECH-34206, Proceedings of the ASME Design Engineering Technical Conferences. 7

[17] Frischknecht, B. D., Howell, L. L., and Magleby, S. P., 2004. "Crank-slider with spring constant force mechanism." No. DETC-2004-MECH-57318, Proceedings of the ASME Design Engineering Technical Conferences. 7

[18] Parkinson, M. B., Howell, L. L., and Cox, J. J., 1997. "A parametric approach to the optimization-based design of compliant mechanisms." No. DETC-1997-DAC-3763, Proceedings of the ASME Design Engineering Technical Conferences. 7

[19] Taguchi, G., 1986. *Introduction to Quality Engineering*. Krauss International Publications, White Plains, NY. 7

[20] Shoemaker, A. C., Tsui, K. L., and Wu, C. F. J., 1991. "Economical experimentation methods for robust design." *Technometrics,* **33**, pp. 415–427. 7

[21] Otto, K. N., and Antonsson, E. K., 1999. "Extensions to the taguchi method of product design." *ASME Design Theory and Methodology,* **DE-Vol. 31**, pp. 21–30. 7

[22] Parkinson, A., Sorensen, C., and Pourhassan, N., 1993. "A general approach for robust optimal design." *ASME Journal of Mechanical Design,* **115**, pp. 74–80. 7

[23] Simpson, T., Poplinski, J., Koch, P., and Allen, J., 2001. "Metamodels for computer-based engineering design: Survey and recommendations." *Engineering with Computers,* **17**, pp. 129–150. 8

[24] Wittwer, J. W., Baker, M. S., and Howell, L. L., 2006. "Robust design and model validation of nonlinear compliant micromechanisms." *Journal of Microelectromechanical Systems,* **15**, p. 33.41. 8

[25] Bechert, D. W., Bruse, M., Hage, W., van der Hoeven, J. G. T., and Hoppe, G., 1997. "Experiments on drag-reducing surfaces and their optimization with an adjustable geometry." *Journal of Fluid Mechanics,* **338**, pp. 59–87. 8

[26] Olsson, H., Astrom, K. J., de Wit, C. C., Gafvert, M., and Lischinsky, P., 1998. "Friction models and friction compensation." *European Journal of Control,* **4**, pp. 176–195. 8

[27] Boyle, C., Howell, L. L., Magleby, S. P., and Evans, M. S., 2003. "Dynamic modeling of compliant constant-force compression mechanisms." *Mechanism and Machine Theory,* **38**, pp. 1469–1487. 8

[28] Bhatti, M. A., 2006. *Advanced Topics in Finite Element Analysis of Structures*. John Wiley. 15

Appendix A

Using the Analysis Code

A.1 Introduction

This appendix provides a description of the source code used to obtain the results found in the body of this thesis. It is not intended to give a thorough development of the finite element theory, or the optimization theory. The intent is that this appendix will aid the user in understanding the flow of the code, and how to use it to design constant-force mechanisms. The code is written specifically to design one configuration of constant-force mechanisms. It is hoped that the code can be useful for other purposes, but extensive testing has not been done and some features not often used for constant-force mechanism design may not be functional. Section A.2 illustrates a problem definition to show what type of engineering problem can be solved. Section A.3 explains how to configure the code to solve the problem.

A.2 Problem Setup

This section discusses step by step how to set up a constant-force mechanism problem so that it can be solved by the code. The variables and parameters that need to be specified are found at the beginning of the main.m file and are labeled below as they are labeled in the program.

1. The first step is to select a starting design defined by nodal coordinates. The first node will automatically have a fixed boundary condition. If another boundary condition is desired the prepFEA.m file must be changed. The nodal positions are entered in the X and Y vectors.

2. The second step is to specify the contact node with the applied displacement, and define the cam profile. The contact node is located by specifying how many nodes (n) are between it and the fixed node. The cam profile is defined by specifying the cam constants: cam_rad, $Xcent$, $Ycent$, a, and b. It's possible to restrict a and b in the optimization later to use only circular cams.

3. The third step is to specify material properties E, Pr, and mu (if friction is necessary), with cross sectional dimensions h and b.

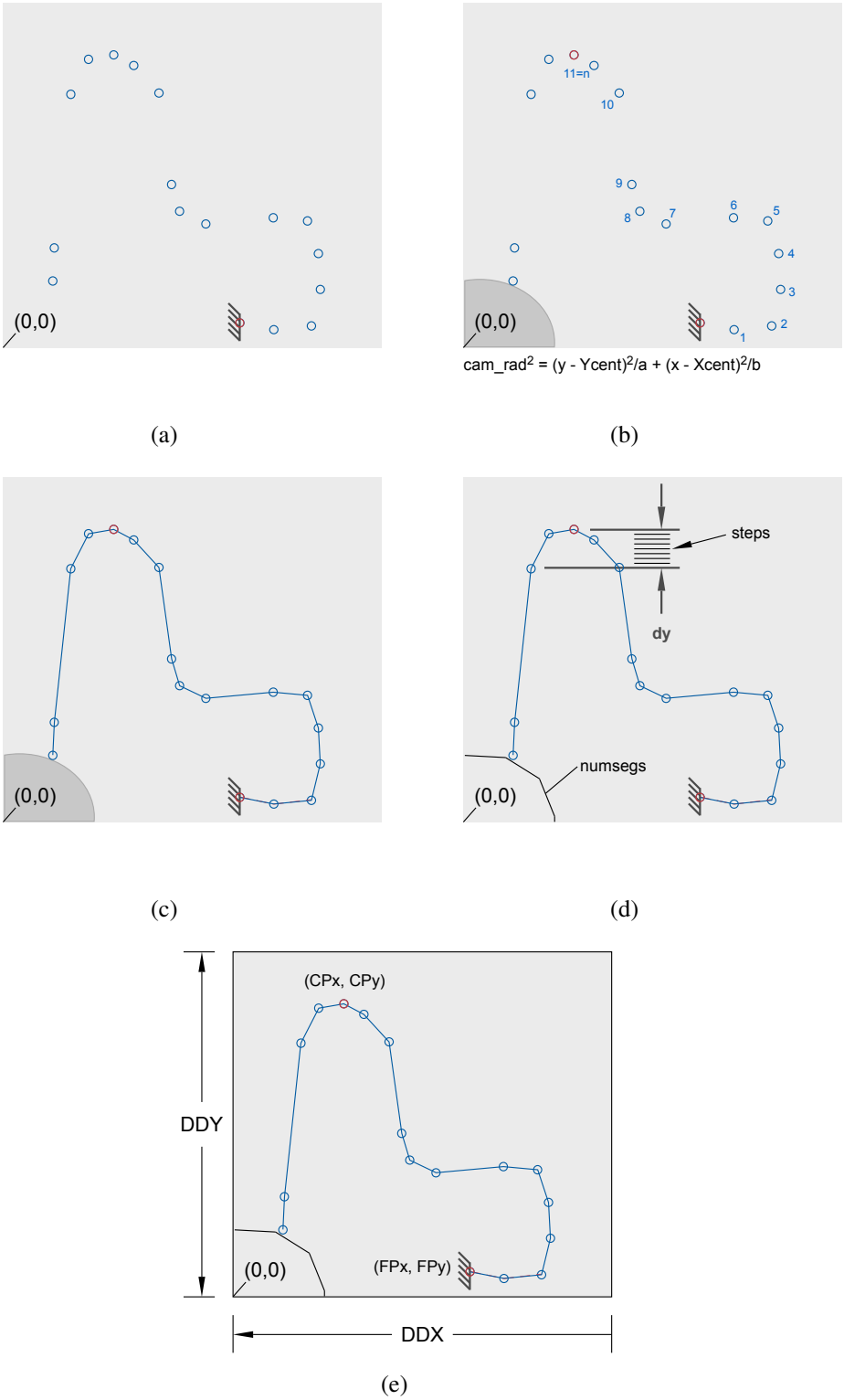

Figure A.1: Steps in the problem definition. (a) Define nodes. (b) Define contact node and cam profile. (c) Define element and material properties. (d) Define FEA parameters. (e) Define optimization parameters.

4. Step four is the finite element setup. The load (dy) must be specified, and the number of substeps ($steps$) needs to be specified. The preload is set to be a fraction of the total load (dy). If the preload is between two substeps the constant-force function will use the higher deflection substep. *ASteps* is a parameter used only if there is an interference fit. It adds additional substeps so that the assembly caused deflection can be calculated, and the increase in the preload deflection can be applied. It must be an even number because the steps are divided equally between the two calculations. $Force\_tol$, $Disp\_tol$, and max_iter are values to set convergence criterion, and limit the number of Newton-Raphson iterations in the analysis code. The value for $intFact$ should be less than or equal to one. This value is the fraction of interference that is removed with each iteration of the Newton-Raphson process. Removing the entire interference in one iteration may cause convergence problems. The number of segments used to approximate the cam surface is set with *numsegs*.

5. The final step is to specify parameters for the optimization and Monte Carlo routines. If no optimization is being done on the design, and the finite element analysis is all that is needed, this step can be skipped. For the optimization to work the contraint limits need to be specified. These limits are evaluated using the following parameters:

   - the location of the fixed node (FPx and FPy)
   - the location of the interface node (CPx and CPy)
   - the design domain dimensions (DDX and DDY)
   - the yield stress of the material (Ys)
   - all the values in the 'Constraint Parameters' section of main.m.

   If a surrogate model optimization is used the trust region needs to be defined, which is the design space around the starting design that is used to develop the model. Generally a trust region larger than the tolerance window is used initially. After each optimization run the trust region is decreased until it matches the tolerance window. The initial size and the rate of decrease can be controlled with the parameters $fact1$ and $factdecrate$ respectively.

   The Monte Carlo simulation also relies on special input parameters. The manufacturing tolerances are entered assuming that the tolerance is plus or minus the value entered. All length or position tolerances, such as the nodal coordinates and the cam radius, are taken from the variable *var_X* with the exception of the cross sectional dimensions which are specified as *var_b* and *var_h*. The material properties tolerances are specified as *var_E* and *var_Pr*. Finally the number of samples in the Monte Carlo simulation is specified as *MC_runs*.

These are the basic values needed to define the engineering problem. The next section explains how to run the program, and what output is available.

A.3 Running the Program

The program is run by selecting the appropriate options in the main.m file and then running the file. This section explains what options are available and how to configure the code to run the available routines.

A.3.1 Module Options

```
%%%%%%%%%%%%%%%%%%%%%% Module Options %%%%%%%%%%%%%%%%%%%%%%%%%%%%%%%%
% enter 0 for module 'off'  enter 1 for module 'on'

optimize_on = 0;        % Turns on the optimizer for robust design
generate_x0 = 0;        % Generates a semi-feasible design
opt_x0 = 0;             % Optimizes the initial design w/o robustness
run_ansys = 0;          % Uses ansys to evaluate the final design
run_MonteCarlo = 0;     % Does a Monte Carlo simulation on final design
plot_results = 1;       % Creates figures
```

Figure A.2: The Module Options Section of main.m

These options control which functions are enabled when the program is running. Entering a 0 disables the function, while a 1 enables the function. When *optimize_on* is enabled the program will run one of the available robust optimizations listed in the 'Optimization Parameters' section of the main.m module. The Opt_X0 option enables the deterministic optimization function. If both options are enabled the deterministic optimization is run first, and the results are used as a starting point for the robust optimization. If neither option is enabled the finite element analysis is run on the starting design. The *run_ansys* option executes the ANSYS finite element program in batch mode using the current geometry coming from the optimization routines if they are enabled. The *run_MonteCarlo* option runs the Monte Carlo simulation on the current geometry coming from the optimization routines. The *plot_results* option tells Matlab to generate figures of the results.

A.3.2 Optimization Parameters

These options control the deterministic and the robust optimization routines. The *robust_type* option is used to select between various robust optimization methods. The $func\_evals$ parameter sets the maximum number of objective function evaluations done by the robust optimization routine. The $term\_val$ is a target value for the objective function. Once the objective function reaches that value it will no longer evaluate the function which terminates the optimization. This is used primarily to avoid a long computation time while the objective converges to within a small tolerance. The two parameters $X0\_evals$ and $X0\_term$ do this for the deterministic optimization routine, they respectively control the

```
%%%%%%%%%%%%%%%%%%%%%% Optimization Parameters %%%%%%%%%%%%%%%%%%%%%%

robust_type = 3;        % Specifies the method used for robust analysis
                            % 1 = Monte Carlo  (This function is currently
                                % not fully functional)
                            % 2 = Forward Difference (This function is
                                % currently not fully functional)
                            % 3 = Surrogate Model
                            % 4 = Mating Condition
func_evals = 1000;      % Number of function evaluations for robust opt.
x0_evals = 2000;        % Number of function evals for deterministic opt.
x0_term = -0.99;        % Termination value for deterministic optimization
term_val = -0.99;     % Termination value for robust optimization
w1 = 1;                 % Weight of first objective
w2 = 1;                 % Weight of second objective
```

Figure A.3: The Optimization Parameters Section of main.m

maximum number of evaluations and the value at which the optimization terminates. For multiobjective optimizations the weight factors are controlled with $w1$ and $w2$.

A.3.3 Additional Functions

Several available functions in addition to those described above may be useful. Time estimates are available for modules that have a high computation time. These estimates can be turned on by setting the *tic_on* parameter to 1 or turned off by setting it to 0. The estimate can be updated with every function evaluation in the module that is running or it can be updated less frequently to lower the computation time. The frequency is set with the *inc_count* option, where a higher integer corresponds to fewer time estimate evaluations.

To decrease the computation time parallel processing can be used (this feature may not be functional in all versions). The parallel processing works by creating new directories (nodes) and opening an instance of Matlab in each directory. Text files are created and used to communicate between the various nodes. The driving program will create instructions for each node and wait in a loop until the nodes each finish the instructions and respond. Before it finishes the main program will close Matlab in each node.

A.3.4 Solution Output

The output from the program depends on what options are enabled. Three figures are automatically generated. The first shows the geometry of the design resulting from the deterministic optimization if it's enabled or the starting design if it's not. The second shows the geometry and deflected position of the design from the robust optimization if that option is enabled. The third figure shows the force-deflection curve of the design and includes the compression and expansion curves if a fricitonal coefficient (*mu*) is specified.

A fourth figure can also be generated showing a histogram of the constant force percentage C if the Monte Carlo simulation is enabled.

In addition to the figures, the finite element analysis results of the final design are output to the command window. These results are listed below.

- The deflection of each node (DOF) is given, organized first by node number, then by direction. For example, the first three values in the vector are the x displacement, y displacement, and z rotation of the first node respectively, and the next three numbers are the same for the second node.
- The reaction forces are given in the x direction ($Forcex$) and y direction ($Forcey$) to the applied deflection at each substep.
- The increments of applied deflection (including assembly deflections) are given for each substep. Deflections applied in the x direction are given as the $dispx$ vector, and those applied in the y direction are given as the $dispy$ vector. If no interference occurs these vectors can created by evenly dividing the applied deflection into the correct number of substeps. For the mechanisms presented in this thesis the $dispy$ vector was used with the $Forcey$ vector to create the force-deflection relationship.
- The internal stresses ($Stress$) at the final fully deflected position are given. These stresses are given as axial, shear, and bending stresses in the first second and third columns of the $Stress$ output respectively. Each row in the column gives the data for one element in the finite element model.
- Information is given concerning singular matrix errors ($errSing$) and substeps that did not converge ($notConv$). If $errSing$ is one then the analysis terminated because of a singular matrix error. If some substeps did not converge $notConv$ will list the substeps, the iteration number, and the convergence criteria.
- The normal force at the cam surface is given for each substep in the vector Nf
- The constant force percentage is given as J
- The weighted sum aggregate objective function for frictional analysis is given as Jf if mu is not zero.
- The time taken for all the individual processes is given as $time$.

Other output coming from various functions can be made available. Each function can be called separately to get the output. For example the optimization constraints function (constraint.m) can be called to create a vector C which in this case represents the values of all the constraint functions. This could be used to check the feasibility of any design.

All the various functions take as input values a vector x and a vector $params$ with the exception of the finite element code ('nlfea.m'). These vectors are created from the inputs provided during the problem definition, and are all that are required to run any function. For the finite element code the inputs can be generated using the prepFEA.m function.